AD NUMBER

AD863062

LIMITATION CHANGES

TO:

Approved for public release; distribution is unlimited.

FROM:

Distribution authorized to U.S. Gov't. agencies and their contractors; Critical Technology; OCT 1969. Other requests shall be referred to U.S. Army Aviation Materiel Laboratories , Fort Eustis , Virginia 23604. This document contains export-controlled technical data.

AUTHORITY

USAAMRDL ltr, 23 Jun 1971

AD

USAAVLABS TECHNICAL REPORT 69-43

STUDY AND EVALUATION OF DIRECTED GLASS FIBER REINFORCED PLASTIC HELICOPTER TAIL ROTOR ASSEMBLY

By

Paul F. Maloney
Frank B. Clark
Hugh N. McIntyre

October 1969

U. S. ARMY AVIATION MATERIEL LABORATORIES
FORT EUSTIS, VIRGINIA

CONTRACT DA 44-177-AMC-306(T)
KAMAN AIRCRAFT DIVISION, KAMAN CORPORATION
BLOOMFIELD, CONNECTICUT

DEPARTMENT OF THE ARMY
HEADQUARTERS US ARMY AVIATION MATERIEL LABORATORIES
FORT EUSTIS, VIRGINIA 23604

This program was carried out under Contract DA 44-177-AMC-306(T) with Kaman Aircraft Division, Kaman Corporation.

The report describes the results of a program to determine the feasibility of fabricating a tail rotor assembly from fiberglass reinforced plastic materials. Included is a study of techniques for automating the fabrication processes.

The report has been reviewed by the U.S. Army Aviation Materiel Laboratories and is considered to be technically sound. It is published for the exchange of information and the stimulation of future research.

Task 1F162203A14176
Contract DA 44-177-AMC-306(T)
USAAVLABS Technical Report 69-43
October 1969

STUDY AND EVALUATION OF DIRECTED GLASS FIBER REINFORCED PLASTIC HELICOPTER TAIL ROTOR ASSEMBLY

KAMAN AIRCRAFT REPORT NUMBER R-774

by

Paul F. Maloney
Frank B. Clark
Hugh H. McIntyre

Prepared by

KAMAN AIRCRAFT DIVISION, KAMAN CORPORATION
BLOOMFIELD, CONNECTICUT

for

U. S. ARMY AVIATION MATERIEL LABORATORIES
FORT EUSTIS, VIRGINIA

SUMMARY

The results of further study and evaluation of a new design concept for helicopter tail rotors are reported herein. The original development and evaluation was previously reported in Reference 1. The evaluation was conducted by means of a whirl test which included separate runs at full pitch (19°), overspeed to 110% rpm, and simulated forward flight to 105 knots. The dynamics of this rotor mounted on an Army helicopter and the techniques for automating its production were subjects of separate study phases of this program.

In the course of this and the previous program, sufficient developmental work has been accomplished to demonstrate not only that the basic concept is feasible but that the rotor built in this program is capable of surpassing many of the more rigorous substantiation requirements of operational helicopter rotors. Also, techniques are available for the volume production of such a rotor to high-quality standards at low cost.

TABLE OF CONTENTS

LIST OF ILLUSTRATIONS

LIST OF TABLES

LIST OF SYMBOLS

D	Damping coefficient
e	Effective lag hinge offset of rotor, ft
F	Dissipation energy, ft-lb
$F(t)$	Time-dependent forcing function, ft-lb
g	Acceleration of gravity, ft/sec^2
i	Blade number (1 or 2)
I_b	Mass moment of inertia of rotor blade about effective lag hinge, slug ft^2
k	Effective spring rate, lb/ft
m	Effective mass, slugs
M	Total effective mass including tail rotor mass, slugs
N_r	Rotor speed, percent
R	Rotor radius, ft
r	Radial coordinate of blade
S_b	First mass moment of blade about effective lag hinge, slug ft
t	Time, sec
T	Kinetic energy, ft-lb
U	Potential energy, ft-lb
x,y	Coordinates relative to axes passing through static position of rotor hub; x-axis parallel to ground and positive forward, y-axis perpendicular to ground and positive upward, ft
θ_o	$\zeta_1 + \zeta_2$, rad
θ_1	$\zeta_1 - \zeta_2$, rad

ζ	Blade lead angle, rad
ψ	Rotor azimuth position, Ωt, rad
Ω	Rotor speed, rad/sec
ω_b	Blade in-plane natural frequency, $\sqrt{\frac{K_b + e S_b \Omega^2}{I_b}}$, rad/sec

Subscripts

b	Blade
i	Blade number (1 or 2)
p	Pylon
x	In horizontal direction
y	In vertical direction

Dots over symbols denote differentiation with respect to time.

INTRODUCTION

This report presents the results of further study and evaluation of the directed glass fiber reinforced plastic tail rotor, the original development of which was reported in Reference 1. The program reported herein consisted of supplementtal whirl tests, further dynamic analysis, and a study of fabrication techniques applicable to volume production of consistent high quality.

Whirl testing included separate runs with full pitch, overspeed, and simulated forward flight with sufficient instrumentation to determine critical loadings for all test conditions. The recorded loadings are presented together with an evaluation of their significance.

In the dynamic analysis, the application of a rotor of this type to a flight vehicle was investigated. The analysis was particularly concerned with tne more unique characteristics of the rotor and the effect that these might have in a practical aircraft application. The study of fabrication techniques was aimed at the development of a process that would yield a high level of production automation so that uniformly high quality could be maintained at minimum cost per unit.

The results of all of the above effort are presented in this report, as are recommendations for the further development and evaluation of this new concept in helicopter rotors.

WHIRL TEST

An important part of the further evaluation of the directed glass fiber tail rotor involved supplemental whirl testing of the prototype rotor at the contractor's whirl test facility. This facility, in addition to having the capability of turning the rotor at the desired rotational speed and the ability to change the blade pitch setting, can simulate forward flight operation as well. This is accomplished by the juxtaposition of an open-end wind tunnel such that the tunnel exhaust passes over the tail rotor disc in an edgewise direction, thus simulating forward flight airflow. The general arrangement of the tail rotor whirl test facility is shown in Figure 1.

Testing in this program,which included separate runs at full pitch (19^{o}), overspeed (110%), and simulated forward flight to 105 knots, was accomplished in approximately 10 hours of operation. This testing made use of the prototype rotor which had previously been whirled for 25 hours as reported in Reference 1. This rotor has therefore completed a rather extensive series of tests which provide ample demonstration that the concept is indeed practical and has good potential for broad application. In the course of the prior endurance whirling, minor problems with the blade construction were uncovered, and modifications were incorporated to correct these before initiation of the supplemental testing. A description of these changes and the whirl test results follows.

ROTOR MODIFICATION

In the course of the 25-hour endurance whirl test of this rotor, certain minor quality problems became evident, as reported in Reference 1. The more significant of these was the appearance of an incipient bond void at the aft edge of the leading edge ballast weight. A secondary problem was tip cap delamination. Consequently, modifications of the rotor were undertaken to eliminate these difficulties. Figure 2 depicts the rotor assembly and indicates blade components and radial stations of note.

Removal of the leading edge consisted of disecting the wrap. A spanwise cut was made directly behind the leading edge weight from Station 14.75 to the outboard end of the blade. A chordwise cut was made at Station 14.75, freeing the ballast weight from the blade. The remaining leading edge wrap was carefully removed by hand-peeling 2-inch-square sections from the blade. Extreme care was excercised to minimize damage to the glass fiber epoxy skin laminate covering the honeycomb core.

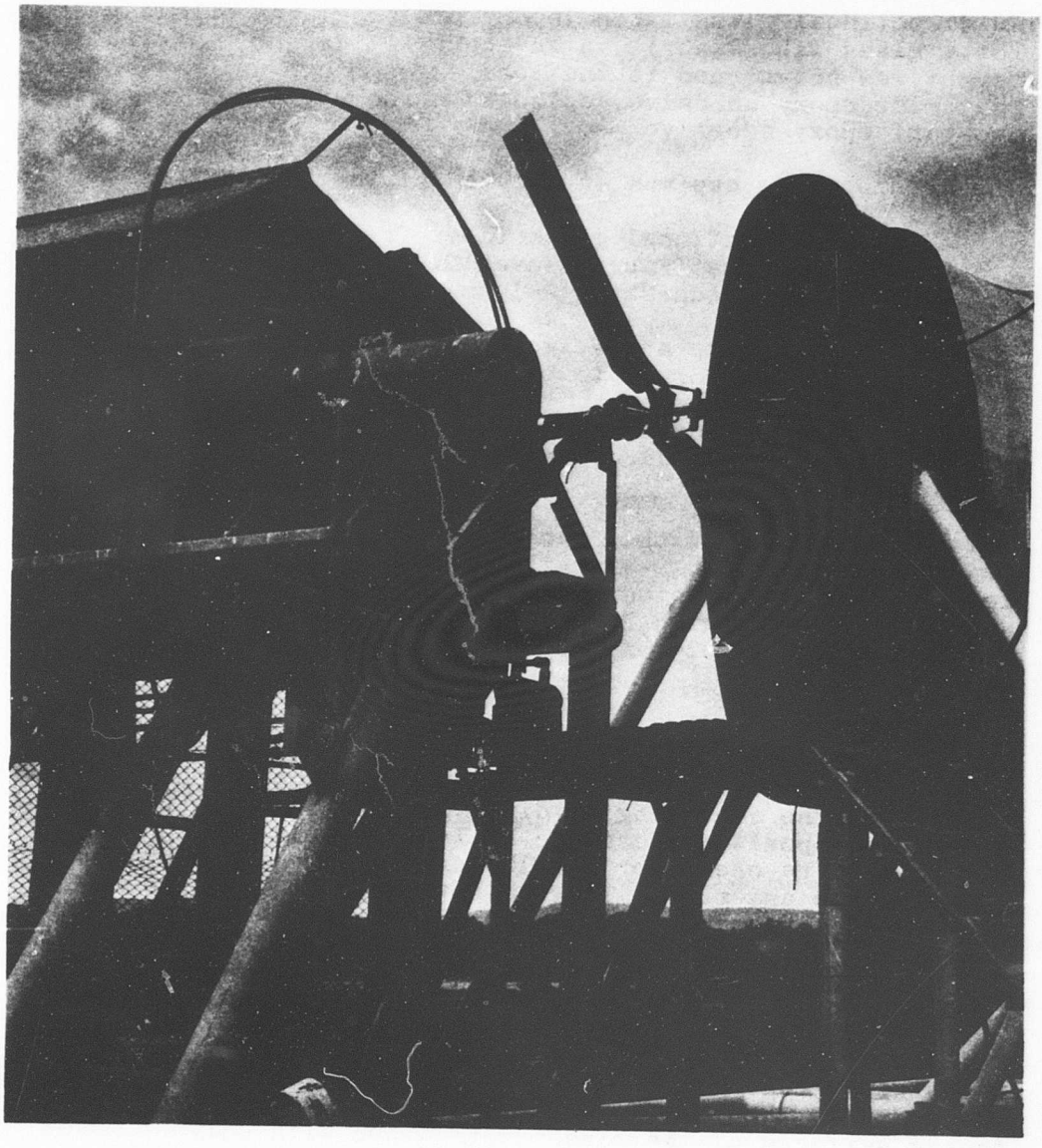

Figure 1. General Arrangement of Tail Rotor Whirl Test Facility.

The adhesive layer between the leading edge cap and the fiberglass blade skin was carefully removed by hand sanding with #320 grit paper.

To improve the leading edge structurally, crossplied (± 45°) unidirectional glass fiber (epoxy pre-preg) was substituted for a glass fiber fabric in an epoxy wet lay-up. The ballast weight was hot-bonded to the leading edge cap using a modified polyamide-epoxy adhesive, replacing a room-temperature-curing two-part epoxy adhesive.

The leading edge cap was fabricated of the following materials:

Unidirectional glass fiber Pre-Preg (Epoxy)
#120 Glass Fabric Woven Pre-Preg (Epoxy)
FM-1000 Adhesive (Polyamide-Epoxy)

The leading edge cap and weight assembly was laid up on a male mandrel, which conformed to blade contour, and was fabricated of a high-temperature epoxy tooling resin. The lay-up consisted of 10 plies of alternately orientated #1002 material 45° to the chordwise direction covered by one-ply #120 glass pre-preg material.

Prior to assembly of the leading edge, the ballast weights removed from the blades were stripped of all adhesive and were degreased, vapor blasted, Alkaline cleaned, water rinsed, air dried, and primed with BR-1009-49 Primer. The primed weights were wrapped in a ply of FM-1000 adhesive, which was heat-tacked in place.

Buildup of the cap consisted of positioning a peel ply and then two unidirectional plies on the mandrel. The ballast weight assembly was positioned on the buildup and heat-tacked in place. The remaining unidirectional plies of stepped widths were positioned on the buildup external to the weight and covered by one layer of #120 pre-preg, which completed the leading edge assembly. The laminate and the mold assembly were vacuum-bagged and autoclave-cured at 320°-330°F for 90 minutes at 50 psi, maintaining full vacuum throughout the cure. On completion of the cure, the assembly was cleaned up, trimmed, and fitted to the rotor blade assembly.

The leading edge assembly was bonded to the blade using a room-temperature-curing two-part epoxy adhesive. The peel ply was removed from the faying surfaces of the leading edges, and the faying surfaces of the blades were wiped with solvent prior to bonding. A uniform coat of adhesive was applied to all faying surfaces. The leading edge was positioned on the blade and

BLANK PAGE

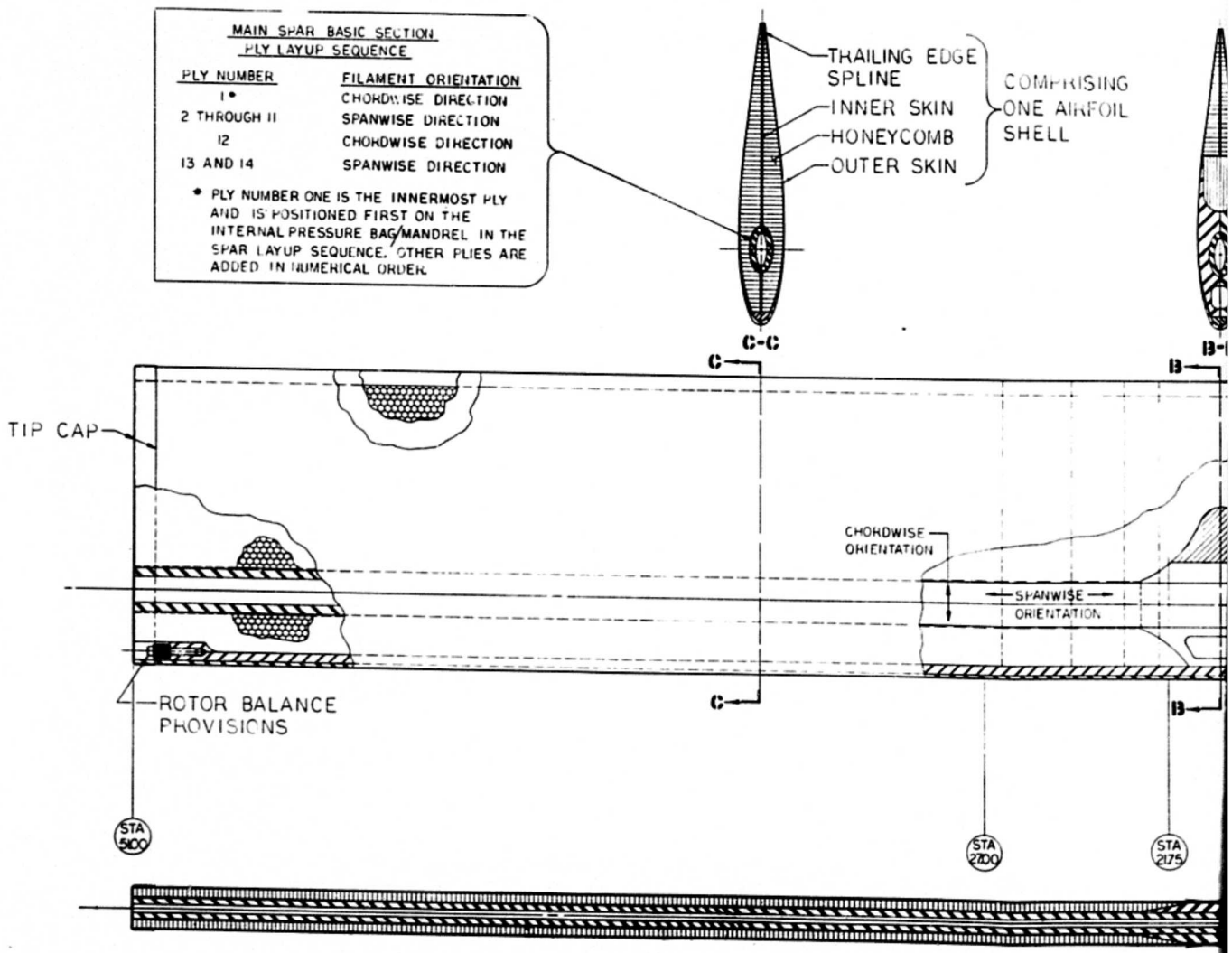

Figure 2. Directed Glass Fiber Reinforced Plastic Tail Rotor Assembly.

A

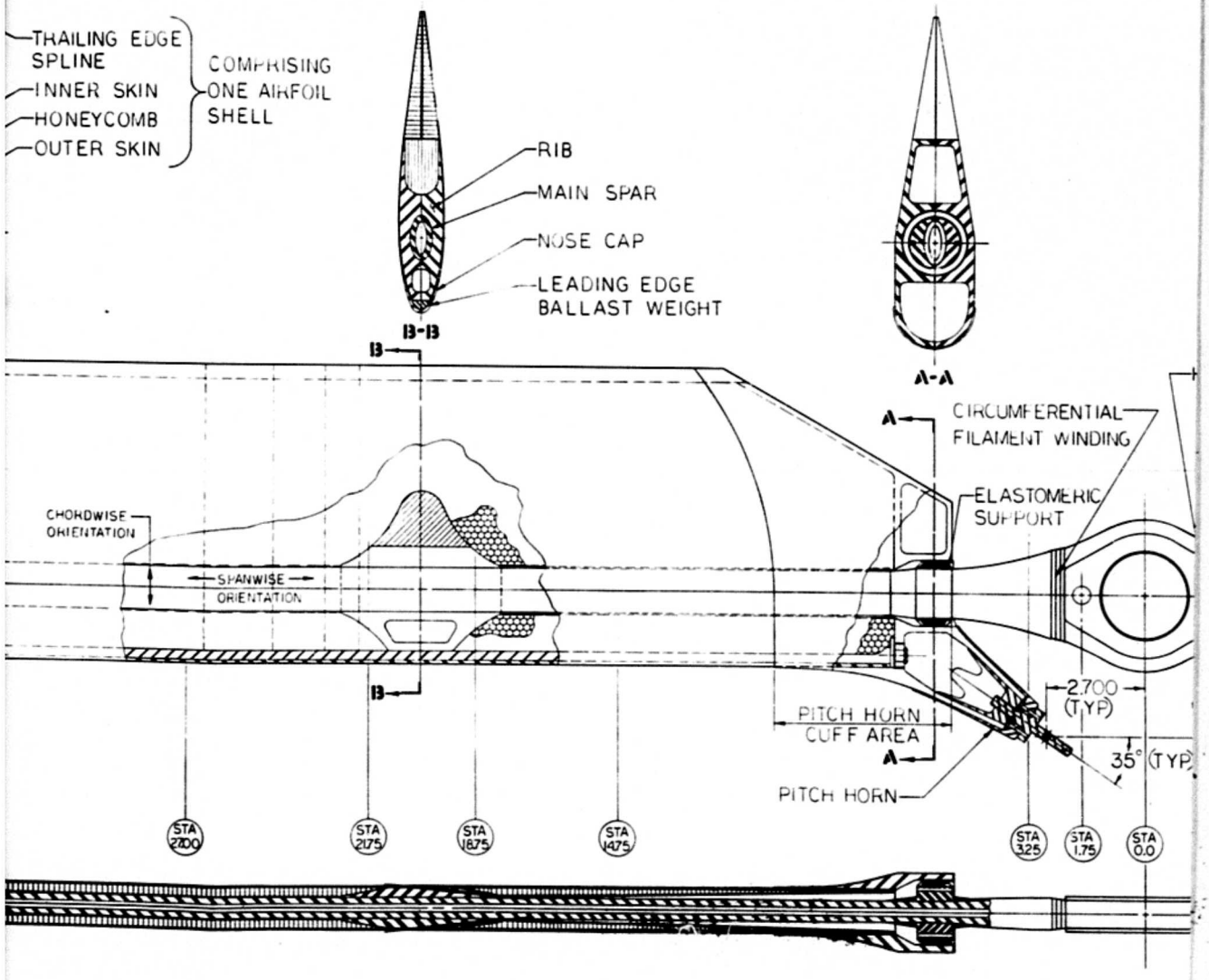
TRAILING EDGE SPLINE
INNER SKIN
HONEYCOMB
OUTER SKIN
COMPRISING ONE AIRFOIL SHELL
RIB
MAIN SPAR
NOSE CAP
LEADING EDGE BALLAST WEIGHT
B-B
A-A
B
A
CIRCUMFERENTIAL FILAMENT WINDING
ELASTOMERIC SUPPORT
CHORDWISE ORIENTATION
SPANWISE ORIENTATION
2.700 (TYP)
PITCH HORN CUFF AREA
35° (TYP)
PITCH HORN
STA 2800
STA 2175
STA 1875
STA 1475
STA 325
STA 1.75
STA 0.0

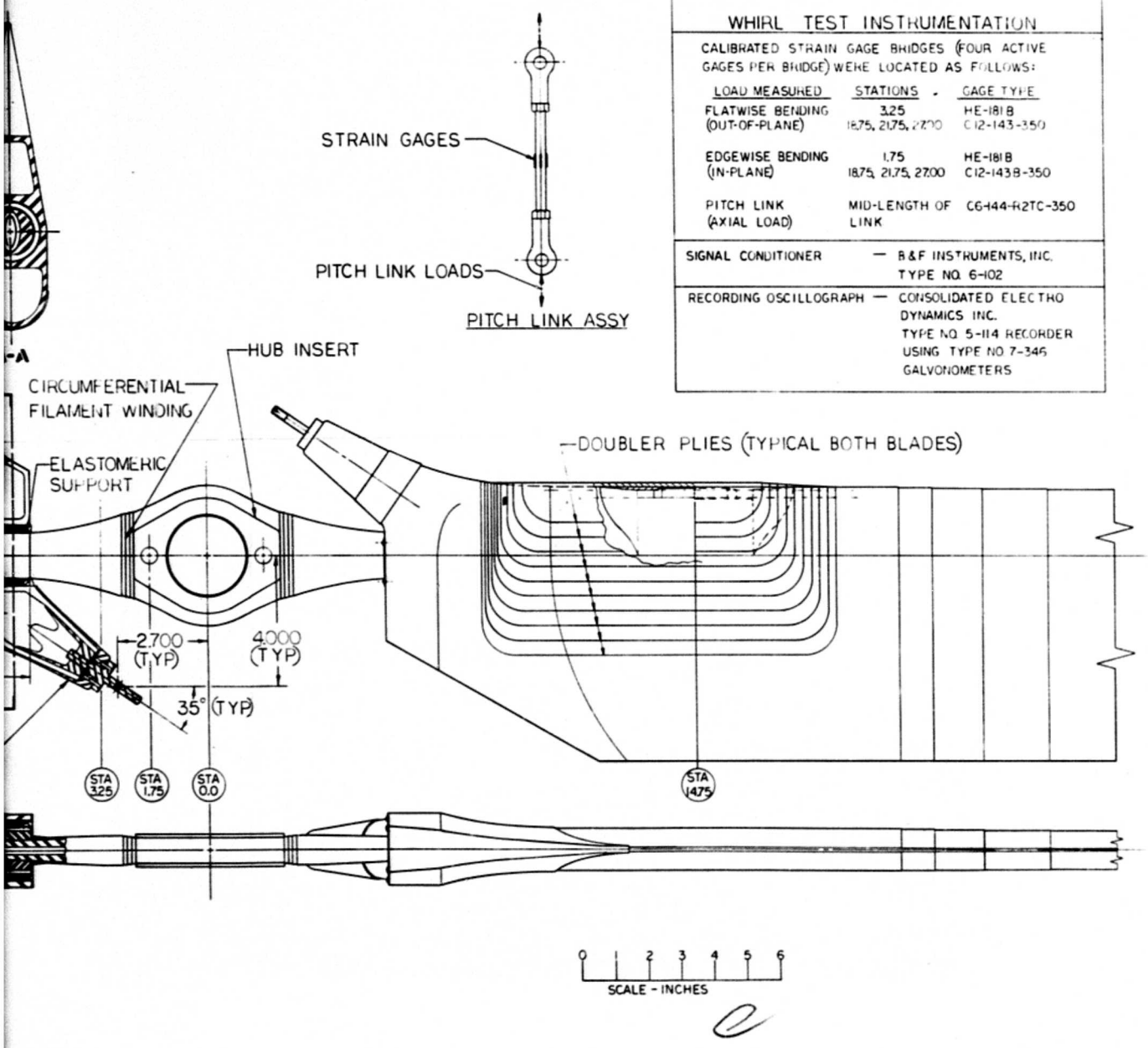

WHIRL TEST INSTRUMENTATION

CALIBRATED STRAIN GAGE BRIDGES (FOUR ACTIVE GAGES PER BRIDGE) WERE LOCATED AS FOLLOWS:

LOAD MEASURED	STATIONS	GAGE TYPE
FLATWISE BENDING (OUT-OF-PLANE)	3.25 18.75, 21.75, 27.00	HE-181B C12-143-350
EDGEWISE BENDING (IN-PLANE)	1.75 18.75, 21.75, 27.00	HE-181B C12-143B-350
PITCH LINK (AXIAL LOAD)	MID-LENGTH OF LINK	C6144-R2TC-350

SIGNAL CONDITIONER — B&F INSTRUMENTS, INC. TYPE NO. 6-102

RECORDING OSCILLOGRAPH — CONSOLIDATED ELECTRO DYNAMICS INC. TYPE NO. 5-114 RECORDER USING TYPE NO. 7-346 GALVONOMETERS

held in place. A vacuum of 20-22 inches of Hg. was maintained during cure. On completion of cure, excess adhesive was removed from the blade, and the edges of the cap were blended to blade contour.

The exposed inboard portion of the leading edge weight was cleaned and primed with EC-1682 primer prior to splicing. A machined half tube was fitted and bonded to the ballast weight halves, with the center of the splice located at Station 14.75. On completion of cure, excess adhesive was removed from the edges of the splice, and it was blended to blade contour.

Ten glass-fabric doubler plies laminated with an epoxy laminating resin were positioned on the blade assembly so as to overlap the old and new leading edges. On completion of the buildup, the doublers were vacuum bagged and squeegeed to blade contour. A vacuum of 20-22 inches Hg. was maintained on the buildup during cure of the laminate. On completion of cure, the inboard doubler buildup was blended to blade contour, thus completing leading edge modification.

Preliminary balance of the rotor was conducted, and excellent balance was achieved prior to tip cap installation. Final tip cap installation consisted of two layers of #120 glass fabric with epoxy resin wet lay-up in place. Recheck of balance revealed that it was still within limits.

SIMULATED FORWARD FLIGHT

In the development cycle of a new rotor, one of the important questions determining the acceptability of the design involves the magnitude of the vibratory loads experienced in forward flight and the ability of the blade structure to withstand these loads. While the means are available for their calculation, the results of such calculations for a highly flexible rotor of the type under consideration cannot be viewed with high confidence in their accuracy. It was therefore considered desirable to determine the vibratory loadings directly by measurement on the tail rotor whirl test facility. An overall view of this apparatus is shown in Figure 1. The structure on the left houses a 200-horsepower electric motor, which powers the rotor and also contains actuators for the control of blade pitch. The structure on the right is an open-end wind tunnel, which contains a 1380-horsepower piston engine and a three-bladed propeller. This system is used to generate a stream of air which completely submerges the tail rotor in an edgewise flow, thus simulating forward flight. Tunnel exhaust velocity is measured and can be controlled

within a range of from 30 to 105 knots. It is therefore possible to gain valuable information as to the flight characteristics of a new tail rotor under controlled conditions at a minimum of risk and expense.

The tail rotor was instrumented with strain gages for the purpose of recording blade load distribution and pitch link load. Since blade vibratory bending was of primary interest, the gages were installed, connected in bridges and calibrated so that bending moments would be recorded directly in terms of inch-pounds of vibratory moment. For flatwise (out-of-plane) bending, Stations 3.25, 18.75, 21.75, and 27.0 were instrumented; for edgewise (in-plane) bending, Stations 1.75, 18.75, 21.75, and 27.0 were instrumented. It was considered that this would give adequate definition to blade vibratory bending distribution and would bracket the primary areas of interest. The pitch links were instrumented and calibrated in such a way as to measure axial loads directly in pounds force. Instrumentation and strain gages are noted on Figure 2.

Since this rotor had previously been whirled without the wind tunnel on the same rig, no special preparations prior to installation were necessary. Initial runup revealed some vibration attributable to rig assembly problems. These problems were isolated and corrected, and the rotor was run to full speed. Loads were recorded at 0, 3, 6, and 9 degrees of blade pitch in a zero wind condition. The open-end wind tunnel was then started, and loads were recorded at 0, 3, and 6 degrees of blade pitch for simulated forward flight speeds of 30, 50, 70, 90, and 105 knots. Because of a limitation in the capacity of the slip ring, the entire series of runs was repeated with a change in hookup, which was necessary to obtain data from all gages.

The vibratory loads recorded during simulated forward flight operation are presented in Table I. The generally low level of the moments is attributable to the low bending stiffness of this design. A gradual progression of the bending moments with velocity and with blade pitch is evidenced, with no rapid digressions or resonances indicated. The rotor operated smoothly throughout the entire forward-flight simulation.

To evaluate the magnitude of these loads, it is necessary to compare them to the strength of the rotor. This can be done with the aid of the fatigue tests that were conducted in an earlier phase of the program and reported in Reference 1. That reference shows the results of three spar fatigue tests at ± 8900 psi. The failure that occurred after 1.09 million cycles at this level was correlated to processing deficiencies which were eliminated. Two subsequent specimens survived 5.0 million cycles of stress at this same level without any signs

TABLE I

ROTOR LOADS DURING SIMULATED FORWARD FLIGHT

Wind Veloc, kn	RPM	Blade Pitch, degs	Flatwise Bending Moments, Inch-pounds Station 3.25	18.75	21.75	27.0	Edgewise Bending Moments, Inch-pounds Station 1.75	18.75	21.75	27.0	Pitch Link Load, lb
0	1733	0	-	± 25	± 31	± 14	± 90	± 48	± 106	± 28	0
0	1733	3	-	± 16	± 31	± 19	± 124	± 72	± 142	± 28	71
0	1733	6	-	± 22	± 31	± 25	-	± 72	± 142	± 57	140
0	1733	9	-	± 25	± 39	± 22	-	± 96	± 176	± 85	197
30	1733	0	-	± 29	± 47	± 28	-	± 96	± 142	± 57	0
30	1733	3	-	± 38	± 39	± 36	-	± 96	± 142	± 85	64
30	1733	6	-	± 41	± 39	± 33	-	± 96	± 178	± 114	133
50	1733	0	-	± 48	± 70	± 41	-	± 96	± 178	± 85	0
50	1733	3	-	± 63	± 86	± 69	-	± 96	± -	± 114	52
50	1733	6	-	± 95	± 118	± 80	-	± 120	± -	± 114	123
70	1733	0	± 29	± 76	± 105	± 66	-	± 120	± 165	± 111	0
70	1733	3	± 2	95	± 141	± 86	-	± 120	± 165	± 139	54
70	1733	6	± 2		± 147	± 105	-	± 120	± 220	± 194	125
90	1733	0	± 30	± 105	± 123	± 105	-	± 167	± 193	± 139	-15
90	1733	3	± 21	± 111	± 164	± 86	-	± 143	± 193	± 222	42
90	1733	6	± 26	± 146	± 223	± 121	-	± 191	± 275	± 277	115
105	1733	0	± 33	± 130	± 168	± 99	-	± 191	± 193	± 166	-22
105	1733	3	± 28	± 155	± 158	± 119	-	± 167	± 220	± 194	15
105	1733	6	± 28	± 250	± 199	± 188	-	± 239	± 303	± 249	88

of failure or deterioration, and tests were terminated at that point. It is therefore considered that ± 8900 psi is a level that can be successfully survived by spars of the present design and that the failure level is higher than this. In the absence of further fatigue test data, the demonstrated run-out level will be used as a base, and the allowable operating stress level will be determined by reducing the S-N curve to account for variability in strength. Since spars made by the techniques developed in this program are expected to have uniformity comparable to that of contemporary metal spars, a typical 25% reduction will be used. The resulting allowable fatigue limit is ± 6670 psi. With this allowable stress and the known spar section properties, the allowable fatigue moments are determined to be ± 583 in.-lb edgewise and ± 303 in.-lb flatwise when each occurs independently. Comparing measured loads to these allowable moments reveals that ample margin exists for all forward-flight speeds. A combination of stresses from flatwise and edgewise moments will reduce the margin slightly; however, section contour and load phasing minimize this effect. Out-board blade sections where the airfoil shell structure is fully effective have substantially higher bending strength and therefore will also operate well below the fatigue limit. The net result of this situation is that no fatigue damage will be accrued in any steady, level, forward-flight condition; therefore, the fatigue life of the rotor will be very high. The only flight conditions which could contribute fatigue damage are the dynamic maneuvers, which by nature are infrequent and of short duration.

The fatigue damage accumulated per flight hour by such maneuvers is extremely low; hence, it is concluded that fatigue life of the rotor will be very high. Table I also presents peak measured pitch link loads recorded during simulated forward-flight operation. These loads are within the operational spectrum of the UH-1D aircraft and present no structural problem. Pitch link loads could be reduced by the incorporation of centrifugal counterweights if such reduction is desirable.

WHIRL TEST WITH FULL PITCH

Table II presents loads recorded during operation at blade pitch angles from zero to full pitch (19^{o}). Loads recorded included two flatwise and two edgewise bending stations as well as pitch link loads.

Data were taken at essentially constant rpm with no wind; however, because of power limitations of the test rig, it was not possible to attain the higher pitch settings at full rpm. The final two increments of blade pitch were reached by starting from a slight overspeed at lower pitch settings. The pitch

TABLE II

ROTOR LOADS FOR PITCH SETTINGS UP TO MAXIMUM, 19°

Blade Pitch, degs	RPM	Wind Veloc, kn	Bending Moments, Inch-pounds				Pitch Link Load, lb
			Flatwise Station		Edgewise Station		
			18.75	27.0	18.75	21.75	
0	1732	0	± 19	± 11	± 96	± 101	0
3	1732	0	± 16	± 19	± 96	± 101	69
6	1732	0	± 16	± 22	± 96	± 126	138
9	1732	0	± 16	± 25	± 96	± 126	192
12	1732	0	± 25	± 22	± 96	± 101	253
15	1713	0	± 41	± 28	± 120	± 152	310
19	1695	0	± 79	± 75	± 96	-	371

TABLE III

ROTOR LOADS FOR OVERSPEED CONDITION

Blade Pitch, degs	RPM	Wind Veloc, kn	Bending Moments, Inch-pounds				Pitch Link Load, lb
			Flatwise Station		Edgewise Station		
			3.25	21.75	21.75	27.0	
0	1543	0	± 10	± 14	± 44	± 27	36
0	1733	0	± 16	± 14	± 89	± 54	39
0	1812	0	± 22	± 22	± 111	± 107	39
0	1856	0	± 29	± 50	± 134	± 107	39
0	1914	0	± 29	± 58	± 134	± 107	39

change mechanism was then actuated at the maximum rate to achieve the higher pitch increments before the rpm decayed below operational levels. The full 19° pitch was reached while the rotor was still in the operational range and only 2% below maximum operating rpm.

Review of the loads recorded shows very little increase of vibratory blade bending with increased pitch. The last two increments that were recorded for a quasi-steady state condition do not depart significantly from the trend of the other data. All vibratory bending moments were well below those encountered in the simulated forward-flight operation and therefore will have no influence on rotor fatigue life. Pitch link load approximates a linear function of pitch angle, since it is derived primarily from centrifugal pitching moment and the elastic properties of the pitch-spring section of the rotor. While the loads shown are not unduly high, it should be noted that their magnitude could be substantially reduced by the incorporation of centrifugal counterweights. Such weights are commonly used, and while they do increase total rotor weight, they do not contribute to complexity nor do they introduce adverse maintenance or reliability considerations.

OVERSPEED WHIRL TEST

As part of the development and substantiation of any new rotor, an overspeed whirl test is usually conducted as a partial demonstration of structural integrity and of the presence of some margin in centrifugal force capacity of the design. The present rotor was designed to the criteria of the UH-1 helicopter and therefore must be able to withstand a 10% overspeed. The maximum normal operating speed for this rotor is 1732 rpm, and the 110% speed is therefore 1905 rpm. To attain this speed on the whirl test rig, a step-up belt and pulley system is introduced in the rotor drive train. Initial operation of the rotor at speeds above the normal operating speed produced vibrations which limited attainable speed. The retightening of all joints and the incorporation of some supplemental rig stiffening eliminated the problem, and the rotor was subsequently run to the overspeed condition without incident.

The maximum rpm sustained was 1914, and the loads recorded for various speeds up to this level are listed in Table III. Here again, a modest trend of blade loads with increasing rpm is noted, with the general levels being quite low. This is as expected for a flat-pitch, no-wind condition. It is also seen that pitch link load remained essentially constant at a very low value for this entire series of runs. As a result of this test, a centrifugal force capacity more than 21% greater than that required for normal operation has been demonstrated for this rotor.

STUDY OF AUTOMATION TECHNIQUES

The rotor that was successfully designed and tested in this program was fabricated by techniques which are described in detail in Reference 1. To a large extent, these techniques involved manual effort, with the aid of a limited amount of tooling, and required the development of an intermediate level of skill. It was recognized early in the program that the quality of the end product could be influenced to a significant degree by various manual steps in the fabrication process. To this end, a number of spar samples were invested in the development of a learning curve, with the result that successive spars did in fact exhibit improved quality and uniformity, as revealed by X-ray inspection and test results. Despite the demonstrated ability to produce an acceptable product by these methods, the problems of assuring a constant high level of quality in series production dictated the need for a study of fabrication techniques that could be automated. The intent of such techniques would be to minimize the manual skill required and to make the final product subject to machine element variability only.

Recent Government-sponsored programs in the area of advanced composite materials have encountered the same basic drawback in state-of-the-art fabrication techniques and, as a result, have been required to pursue the same goals stated above. A review of published results from these efforts was conducted in the hope that some of the techniques developed would be applicable to the fiberglass tail rotor under discussion. Some of the more pertinent and interesting of these techniques are described in References 2, 3, and 4. Each of these utilizes a mechanized transport system for positioning and applying tapes or filaments of the desired material. Most provide for automatic cutoff at the proper length and angle by a tape controlled or programmed actuation of shears or cutoff blocks. These systems are designed and developed for specific application to flat panels or panels of slight, single curvature such as airfoil surfaces for fixed-wing aircraft. The extrapolation of systems of this type to compound curvature and sharper radii is currently under investigation but has not as yet produced results that are entirely satisfactory. Discussions with the material suppliers and their representatives who provide consulation and technical services in the design and application of automatic tape-laying heads and tape transport systems reveal that quantity production of components with rapid contour change and compound curvature cannot be scheduled until further exploratory and developmental work is completed.

DESIGN CONSIDERATIONS

One of the most significant findings of the fabrication development work performed in this program has been the importance of tension applied to individual tapes during spar fabrication. Final spar quality was found to depend strongly on this feature, and therefore it was considered mandatory that some means of tensioning plies during spar layup be provided in any automation technique to be considered. Another area that presented some difficulty during fabrication development was the complicated hub-transition area. The basis for this design was a consideration for retaining the maximum number of existing components in the tail rotor area and modifying only the rotor. This decision has been reevaluated in the light of work accomplished in this program and other basic design considerations. With the aid of this additional experience, it now is considered prudent to modify the rotor hub area in order to achieve a more balanced design. Such a design would favor the highly loaded spar fibers and permit a straight through path for the blade to blade connection. This change could be accommodated by either modifying the rotor shaft so that it would terminate in a wide clevis or by providing a supplementary fitting which would mount on the present shaft and provide the clevis connection. The rotor spar elliptical section would remain constant, passing straight through the clevis. Supplementary material added to the outside of the spar would accommodate the necessary attachments for a trunnion, which, aligned on a transverse axis through the clevis, would provide the teeter freedom. The tail rotor pitch control rod, coaxial with the rotor shaft, would terminate at its outboard end in a crossbar, each end of which would join to a pitch link. Each link would in turn, be connected to a blade pitch horn. This design favors the highly loaded rotor centrifugal force path while somewhat complicating the more lightly loaded rotor shaft torque and thrust paths. Control rod geometry would be basically the present configuration.

With this design, the spar material would be provided a load path from blade to blade with no digressions and a minimum of stress concentration. In addition to these design and structural benefits, spar fabrication would also be greatly enhanced, and the opportunities for automation would be improved.

In view of these considerations and the total background to date, studies were undertaken to design tools and to devise methods for the automated production of the fiberglass tail rotor. Because of the singular importance of the spar in this design, the automation of its fabrication was the primary goal of the study, with secondary attention given to the airfoil shells and other subassemblies. The results of these studies follow.

AUTOMATION PROCESS OF SPAR FABRICATION

The design of a production tail rotor spar of directed glass fibers will be based primarily on the fabrication methods developed in the course of the present program. The production spar will be a monolithic structure of directed glass fibers in an epoxy matrix with a constant elliptical hollow cross section the entire length of the spar. The spar must be capable of maintaining high tensile loads in a spanwise direction and have low torsional stiffness. Repeatability and reliability of the process are prime considerations to ensure minimum variation in mechanical properties, fabrication cost, fiber distorsion, and uniform torsional stiffness.

A survey of automated processes for the fabrication and cure of plastic reinforced glass fiber structures concluded that at the present time and in the foreseeable future, no equipment is available which is suitable for fabrication of this particular spar. Standard processing methods such as hand lay-up of pre-preg materials, the spraying of chopped fibers, contact molding, matched metal die molding, and pressure bag molding are not suitable because of the rigid dimensional and mechanical requirements of the dynamic spar structure, requiring the ultimate mechanical properties of directed glass fiber epoxy laminate. Based on the above requirements, the automated methods for fabricating the spar narrowed down to the three following possibilities:

1. Filament winding of the spar assembly using an epoxy resin impregnated glass roving.

2. Mechanized applicator of pre-preg unidirectional tapes.

3. "Pull-trusion" of pre-preg tapes.

The curing process for the monolithic spar can be performed only in a heated female mold by applying internal pressure to the spar during the cure cycle. This process assures dimensional control and optimum mechanical properties of the laminate.

Of the above three systems, the "pull-trusion" method was selected for fabrication of the spar. A preliminary laboratory evaluation of the method was conducted; the fixture for this evaluation is illustrated in Figure 3. This device adequately demonstrates that this technique leads to a continuous and smooth fabrication process applicable to the spar. Refinement of the various elements of the tooling would be necessary for the fabrication of full-scale components. Following is a breakdown of the advantages and disadvantages of each system considered.

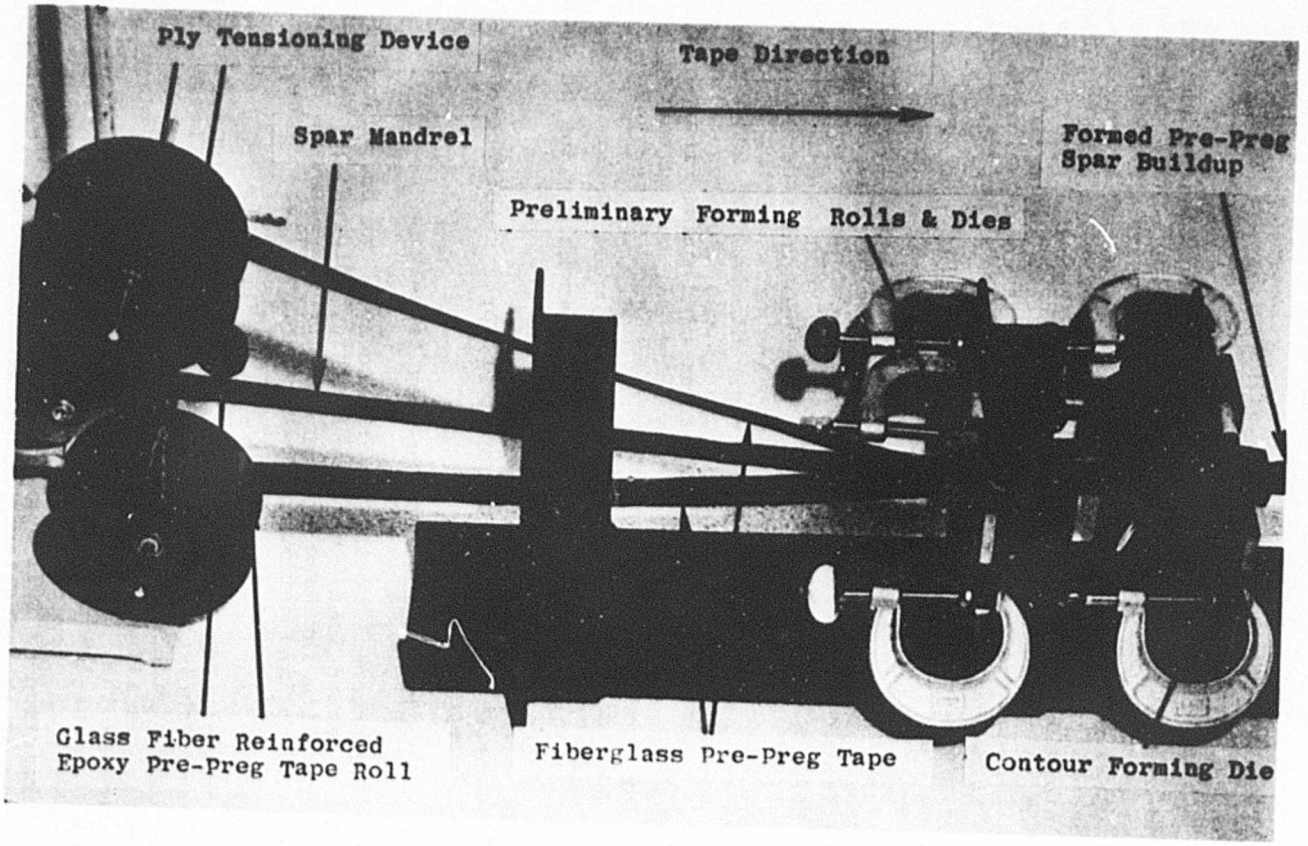

Figure 3. Model for Investigation of "Pull-Trusion" Process for Spar Fabrication.

Filament Winding of Spar Assembly

Advantages

1. The laminate can be fabricated with directional properties.

2. The spar laminate can be produced from a filament of roving preimpregnated material.

3. Excellent repeatability of mechanical properties is attainable.

4. Prestress of filament or roving can be precisely maintained.

5. Orientation of fibers is easily varied on the initial setup, but the established pattern can be accurately controlled.

6. The filament winding process is a completely mechanized process for spar fabrication.

Disadvantages

1. The majority of the directed glass fibers are parallel to the spanwise axis, causing a considerable revision and rework of a standard winding machining.

2. The helically wound glass fibers, wound perpendicular to the spanwise axis, would restrict and cancel the effects of internal spar pressure applied during the curing of the spar assembly.

3. There would be the possibility of excessive resin buildup.

Mechanized Applicator of Pre-Preg Unidirectional Tape

Advantages

1. The mechanism semiautomatically applies and cuts tapes on spar buildup. The unidirectional glass fibers are epoxy impregnated.

2. Excellent reproducibility of properties and fiber orientation is attainable.

3. The tapes can be prestressed to low levels during application.

4. The tape applicator can be adapted to a fully mechanized lay-up of the basic spar structure.

Disadvantages

1. At the present time, only the tape applicator head is available. Considerable development and fabrication time would be required for the tape transport system prior to spar fabrication on an automated production basis.

2. The tape applicator head is designed to handle one given width of tape. Redesign of the applicator to handle the various widths of tapes, as required for spar fabrication on an automated basis, is a possibility, or separate tape applicator heads for the various widths of tapes could be ganged together, whichever method results in greater economy and a smoother fabrication process. In either case, the production fabrication of the spar would be an inherently long process compared to the other methods.

3. Overall cost of this automated machine using the tape applicator would be the highest of the systems evaluated.

"Pull-Trusion" of Pre-Preg Tapes

Definition

Unidirectional and woven preimpregnated tapes are pulled through forming dies or rolls, maintaining uniform high-tension loading on all tapes through the heat-up, forming, and cool-down of the spar lay-up. The lay-up is continuous and is cut to length after forming.

Advantages

1. This is a fully mechanized system; the machine would be designed to meet spar requirements and to comply with prestressing of tapes.

2. Spar cost and fabrication time would be the lowest of all methods evaluated. Fabrication time for the constant cross-section portions of the spar has been estimated at 2 minutes per spar.

3. This method would allow for a continuous in-process inspection of the spar buildup. A run-out of a tape, a loss of tension on a tape, or a defect in the tape would automatically stop the machine.

4. Close control on tolerances and mechanical properties could be maintained by this machine through precise pneumatic control of tape tensions, roll forming pressure, and laminate speed through forming rolls and dies.

Disadvantages

1. To date, no machine of this type has been designed or built to produce a laminate as complex as the monolithic spar development, and fabrication cost may be as high as the programmed tape applicator.

2. Setup time (installation of glass fiber tapes on reels into the machine) is difficult to calculate; however, once the machine is setup, it would run continuously until the tape reels are depleted.

Proposed Spar Fabrication and Preliminary Tool Design of Required Automated Equipment

The monolithic glass fiber spar design consists of the following "B" staged semicured subassemblies: spar structure, with a constant cross-section dimension that is ellipitical and hollow the full length of the spar; hub and transition pads; inboard ribs; and inner races for elastomeric supports. The components would be assembled and cured in a female mold, forming a spar structure. The basic spar ply layup sequence is defined on Figure 2.

1. Automated production of the basic spar structure. Production fabrication of the constant cross-section spar would proceed using a pull-trusion method. Basically, this method consists of pulling unidirectional glass fiber tapes (which are epoxy impregnated and slit to exact widths) through orifices, forming rollers, and dies, resulting in a completed contoured spar lay-up in an uncured state. Fabrication of the spar using directed oriented glass fiber epoxy impregnated tapes and woven glass fiber epoxy impregnated tapes pre-slit to various width requirements would require machine setup time. The setup would consist of installing the tapes in the pull-trusion machine on reels. The tapes are to be strung through feeders, forming rollers, and dies, respectively, in ply widths and glass fiber orientation that comply with the buildup sequence for the monolithic spar. An extruded pressure diaphragm of continuous length can serve as the spar mandrel to which the pre-preg

tapes would be formed and attached. The fabrication of the spar can be a continuous operation limited only by the maximum length of the tape, which is 800 feet at the present time.

The lay-up process would begin on forming the inner spar plies to the pressure diaphragm; this would be accomplished by pulling the diaphragm and plies through respective forming rollers and dies. On reaching Sta. 2, the 2nd spar plies would be adjoined as the buildup passes through the forming rollers and dies of Sta. 2. As the buildup proceeds through the machine, the remaining plies would be fixed to the buildup according to their respective positions in the layup. If forming and tacking the plies together becomes necessary, heat could be applied during the forming of the tapes. Precise control of the tape tensioning would be built into the reels so that all of the individual tapes could be accurately set and adjusted as required. A pneumatic reciprocating drive mechanism would be used to pull tapes at a uniform rate through all rollers and forming dies of the "pull-trusion" machine. Prestressing of the fibers and controlled travel rate through forming dies would ensure uniform tensile stressing of the fibers as they progress through the machine. A clamp device attached to the drive mechanism would lock around and grip the spar buildup on leaving the last forming rollers and die of the outermost ply. On energizing the drive mechanism, the spar buildup would be pulled out of the machine to preset stops, where the spar laminate would then be cut from the "pull-trusion" machine and dropped into a receiving storage bin with protective wrappings to await final assembly and cure. These operations would be fully automatic. On completion of the above spar, the drive mechanism would then return to its starting point and repeat the above cycle.

2. The hub and transition pad, a rectangular block contoured to spar geometry on the inside and tapered on the ends, would be split along the spanwise spar axis into symmetrical and interchangeable segments. The segments would be composed of epoxy pre-preg woven glass fiber cloth and chopped fibers approximately 1/2 inch long. The pre-preg plies and chopped fiber charge, with close control on ply sizes and weight of charge, would be assembled, preheated, preset, and cured to an advanced "B" stage in a modified compression mold. On completion of cure, the pad

would be removed from the mold and stored to await final assembly and cure with the spar.

3. The inboard ribs are designed with a split along the spanwise axis making upper and lower segments which are symmetrical and interchangeable for assembly to the spar. The rib would be fabricated of preimpregnated epoxy chopped glass fibers 1/2 inch long. The chopped fiber charge would be preheated in a modified compression mold, pressed to final dimension, and partially cured to an advanced "B" stage only. At the end of this cure, the rib would be removed from the mold and stored to await final assembly and cure with the spar.

4. The inner races for the elastomeric support are designed with a split along the spanwise axis making upper and lower segments which are symmetrical and interchangeable when assembled to the spar. The races would be composed of glass fibers with impregnated epoxy. These parts would be fabricated using a process similar to that for the inboard ribs.

Final Assembly and Cure of Spar

The spar assembly fixture would be a female mold precisely machined to the spar's outer dimensions, containing cavities for the hub and transition pad, the inboard ribs, and the support races. The spar mold would contain its own heating source and cooling facilities. On cleaning and waxing the mold, the lower segments of the hub and transition pad, the inboard ribs, and the elastomeric inner races would be located in their respective spar mold cavities. All faying surfaces of the component parts to spar bond would be solvent wiped, and a ply of a film adhesive (250°F cure) then positioned on the cleaned surfaces. The spar would be positioned in the assembly mold and attached to component parts, inboard ribs, hub-transition pads, and inner elastomeric bearing races. On completion of assembly, the diaphragm would be connected to the air supply and the mold then closed and locked. The spar assembly would be cured by energizing the self-contained heat elements and the internal spar pressure diaphragm for the prescribed cycle. On completion of cure, the heating elements would be turned off, and the mold then cooled with an integral water system until spar temperature is below 150°F. Self-contained heating elements and cooling coils could cut the time of cure 50%. On reaching 150°F, the spar assembly would be removed from the mold. Visual, radiographical, and destructive testing of samples would then be performed to assure quality performance.

Circumferential Filament Winding, Spar, Transition Zones

The assembly is designed with filament winding in the hub transition area, Sta. 2.25 to Sta. 6.375, with eight wraps of 901 glass fiber yarn, with a layer of #120 fiber glass between successive layers. During the winding process, the filaments and fiber glass are to be coated with a room-temperature-curing epoxy laminating resin. On completion of cure, the spar would be stored for final assembly bond to the airfoil and cuff sections.

THE AIRFOIL SUBASSEMBLIES

The airfoil subassemblies are designed in halves representing either the upper or lower portion of the symmetrical blade as divided by the chord plane. These consist of the airfoil shell with facings of fiberglass, a carved aluminum honeycomb core and trailing edge spline, the pitch horn cuff assembly, and the leading edge cap. Fabrication of these assemblies would follow standard aircraft production procedures for dynamic structure, utilizing an autoclave cure to bond subassemblies.

The pitch horn cuff assembly would be composed of two parts: the outer pitch horn cuff and the internal reinforcing cuff structure. Each half of the cuff assembly representing either the upper or lower portion would be a glass laminate made up of an epoxy pre-preg of directed glass fibers and woven glass fabric. All plies would be template or steel rule die cut to close tolerances. The cuff plies would then be fabricated into a laminate using a female assembly fixture for lay-up and final cure according to a detailed sequence ply buildup chart. The cuff halves could be fully cured using a pressure bag molding process to apply uniform fluid pressure.

The cuff grid, which reinforces the cuff in the area of the elastomeric support is designed to be made up of chopped glass fibers, epoxy resin impregnated. A pre-weighted charge of the pre-preg fibers would be distributed uniformly in a modified compression mold and compressed. The laminate would then be pre-heated, press set, and partially cured. After the laminate is removed from the mold, and reaches room temperature, it would then be stored to await final assembly and cure with the cuff and airfoil components.

Prior to expansion of the honeycomb core, the "hobe" would be contoured to final dimensions with an allowance for the shrinkage of the core in the chordwise direction. On completion of contouring, the hobe is expanded and trimmed to overall length.

Using a location template, the core is then cut for the inboard rib. On completion of the machining operation, the core would be inspected, degreased, packaged, and stored for final assembly.

The airfoil details are then to be placed in a caul assembly mold. The woven glass fabric pre-preg epoxy skin material would be die cut to size for skin and spline plies using a template and a lay-up sequence chart. The first operation would be to locate and lock the pitch horn cuff into the mold and remove the nylon peel ply on the faying surfaces of the cuff. The skin plies "B" stage material are then to be positioned in the assembly caul according to the sequence chart. The inner skin ply, adjoining the core, would be a pre-preg adhesive ply. At the inboard end of the airfoil, the skin and doubler plies would extend to the inboard inner edge of the cuff. The cuff grid assembly would be positioned in the cuff and over the pre-preg plies. The core centers on the spar spanwise axis, butting the cuff grid with one layer of foam adhesive between the grid and the core. The spline pre-preg plies would be locked to the caul assembly fixture. A precured formed epoxy glass fiber laminated inner torsional skin wall, would be positioned on the core, centered on the spar spanwise axis and adjoining the cuff grid inboard end, with one ply of foam adhesive between the core and the skin. This would complete the lay-up of the airfoil subassembly. Cure would then be performed in an autoclave at 250°F for 1 hour at 25 psi.

On completion of cure, the assembly would be cooled to room temperature and machined flat on the chordplane to final dimensions. Surfaces to be machined are the core, spline, and pitch horn cuff. At completion of the machining operation, the airfoil would be removed from the fixture, matched to its opposite half, and inspected and stored for final assembly to the tail rotor blade.

The leading edge cap design is made up of an erosion boot bonded to a structural woven glass fiber laminate with an integrally bonded steel ballast weight. The fiberglass portion of the leading edge cap would consist of an epoxy pre-preg directed glass fiber and a woven glass fiber fabric which would be template or steel rule die cut to close tolerances. To prepare the steel leading edge ballast weight it would be degreased, vapor blasted, primed, and wrapped with one layer of film adhesive.

The assembly of the leading edge cap would consist of lay-up of the cut pre-preg plies on a male assembly mandrel with the ballast weight positioned according to a detailed sequence

buildup chart. Positioning the erosion boot on the buildup would complete the lay-up of the leading edge cap assembly. The lay-up would then be transferred to a female mold, with pressure bag and caul plate, for final cure. The cure cycle of the structure would be 350°F for 1 hour at 70-psi uniform fluid pressure.

A fiberglass U-shaped channel would fit over the leading edge and trailing edge of the cuff to tie the cuff halves together. The channels would consist of woven glass fiber fabric epoxy impregnated plies, steel rule die cut to shape.

The assembly of the cuff channels would consist of positioning the cut pre-preg plies on a male assembly mandrel according to a detailed sequence buildup chart. On completion of the lay-up, the assembly would be transfered to a female mold, with a caul plate and pressure bag arrangement, for final cure. The cure of the structures would be at 350°F for 1 hour at 70-psi uniform fluid pressure.

ROTOR ASSEMBLY

The rotor assembly would consist of bonding the airfoil cuff subassemblies together and to the spar in a caul assembly fixture, vacuum bagging the fixture and caul, and curing in an autoclave with hot air at pressures of 25-30 psi. On completion of the assembly bond, the leading edge caps and the cuff leading and trailing edge channels would be bonded to the assembly, utilizing a bonding fixture to apply localized uniform pressure and heat to the faying surface to be bonded. Intermediate-temperature-curing film-type epoxy adhesive is planned for all of the assembly bonds.

An intermediate-temperature-curing epoxy pre-preg of glass fiber woven fabric of minimum thickness, and epoxy adhesive foam and film material system of low density, would be used for all assembly bonds of the rotor blade. All pre-preg and film adhesive used for the final assembly bond would be template cut according to a cutting-order chart for pre-preg and adhesive plies.

The faying fiberglass surfaces of the cuff airfoil subassemblies would be lightly abraded with #180 grit abrasive paper and solvent wiped prior to assembly lay-up. Peel plies, protecting the faying surfaces, of spar and inboard rib would also be removed.

The cleaned airfoil cuff assemblies would be located in the assembly caul fixture and locked in place. One layer of adhesive and a pre-preg ply are to be positioned in the spar cavity of the subassemblies. A full ply of film adhesive and a pre-preg ply of glass fabric would be positioned on the faying surfaces of the assembly, followed by the spar assembly, which would then be locked in place. The inner steel caps, with a ply of film adhesive on faying surface are then to be positioned on the pitch horn cuff assembly. The assembly buildup would be covered with a full layer of film adhesive, the upper airfoil cuff subassemblies would be positioned on the buildup and locked in place with caul cover plates. The assembly is then to be vacuum bagged and cured in an autoclave. On completion of cure, the rotor assembly would be removed from the mold; cleaned and inspected for integrity of bond, contour, and dimensions.

In preparation for bonding leading edge caps and cuff channels, peel plies are to be stripped from faying surfaces, airfoil leading edges, and cuff leading and trailing edges. One ply of film adhesive would be positioned on the faying surface of the airfoil and cuff. The cuff channels and leading erosion caps are to be located on the buildup and heat tacked in place if necessary. The rotor assembly would then be positioned in the leading edge and cuff curing fixture and heat and pressure applied to the laminate. The cure cycle for this bond would be approximately 160°F for 2 hours at 50 psi. On completion of cure, the assembly would be removed from the bonding fixture; cleaned and inspected for bond quality, contour, and dimensions.

The external steel pitch horn caps are then to be bonded to the assembly using a low-temperature-curing epoxy adhesive. On completion of cure, the pitch horn is to be reinforced with 3 circumferential layers of filament winding with a layer of #120 glass fiber cloth between each winding, which would be wound on the pitch horn, making a 1-inch-wide ring adjoining the outer edge of the steel cap. The filaments and woven fabric would be impregnated with a low-temperature curing epoxy system.

The tip cap would be a glass fiber fabric epoxy pre-preg, which would be compression molded to finished dimensions. The cap would contain an erosion protective boot for the leading edge. The tip cap would be bonded to the blade, utilizing a fixture that would apply heat and uniform pressure to the faying surfaces to cure an epoxy film adhesive at a temperature of approximately 150°F.

INVESTIGATION OF TAIL ROTOR MECHANICAL OSCILLATIONS

An analysis has been conducted to determine the suitability of operating the glass reinforced tail rotor blade on the UH-1D aircraft tail rotor pylon. This analysis, based on the concepts of Reference 5, investigated the nature of the mechanical oscillations resulting from self-excited vibrations, self-excited whirling, and steady force resonance.

THEORY

The equations of motion for a two-bladed rotor on a spring-supported, horizontal axis can be derived with respect to a coordinate system which is fixed in space. With the assumption that the rotor blades possess an effective lag hinge, the coordinates of a mass particle on the blade axis can be determined for each blade from Figure 4. Thus, for blade i,

$$x_i = x - (-1)^i[e\cos\psi + (r-e)\cos(\psi + \zeta_i)]$$
$$y_i = y - (-1)^i[e\sin\psi + (r-e)\sin(\psi + \zeta_i)],\ i = 1,2 \qquad (1)$$

The kinetic energy of blade i is given by

$$T_i = \frac{1}{2}\int_e^R (\dot{x}_i^2 + \dot{y}_i^2)\,dm_b$$

Hence, for constant rotor speed,

$$T_i = \tfrac{1}{2}m_b[\dot{x}^2+\dot{y}^2+e^2\Omega^2+2(-1)^i(\dot{x}e\Omega\sin\psi - \dot{y}e\Omega\cos\psi)]$$
$$+ S_b\{e\Omega(\Omega+\dot{\zeta}_i)\cos\zeta_i + (-1)^i[\dot{x}(\Omega+\dot{\zeta}_i)\sin(\psi+\zeta_i)$$
$$- \dot{y}(\Omega+\dot{\zeta}_i)\cos(\psi+\zeta_i)]\} + \tfrac{1}{2}I_b(\Omega+\dot{\zeta}_i)^2 \qquad (2)$$

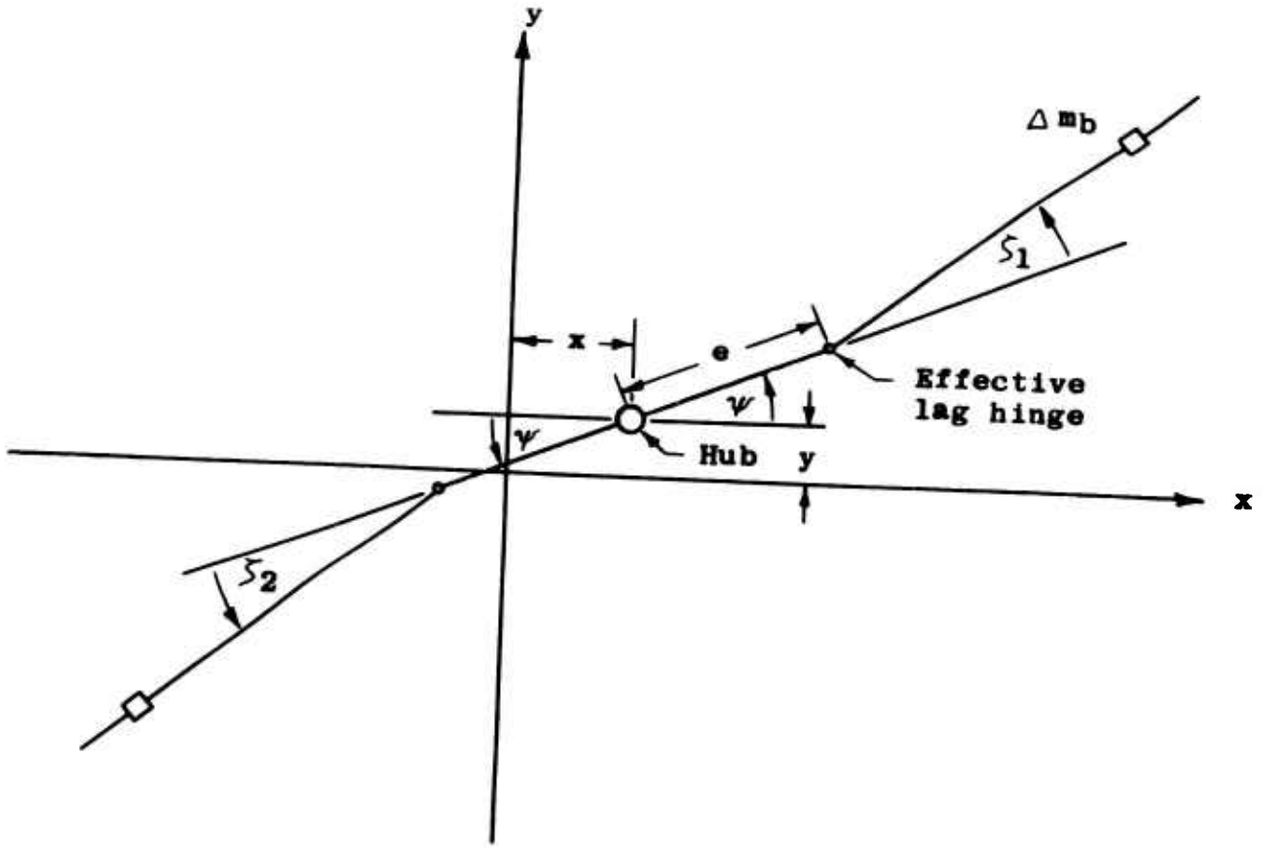

Figure 4. Schematic of Mechanical System Representing Rotor.

The kinetic energy of the pylon is

$$T_p = \frac{1}{2}(m_x\dot{x}^2+m_y\dot{y}^2) \tag{3}$$

The potential energy of the blades and of the pylon can be expressed as

$$\begin{aligned} U_i &= \frac{1}{2}K_b\zeta_i^2 \\ U_p &= \frac{1}{2}(K_x x^2+K_y y^2) \end{aligned} \tag{4}$$

The energy dissipation, or damping, of the blades and of the pylon is given by

$$\begin{aligned} F_i &= \frac{1}{2}D_b\dot{\zeta}_i^2 \\ F_p &= \frac{1}{2}(D_x\dot{x}^2+D_y\dot{y}^2) \end{aligned} \tag{5}$$

The total kinetic, potential, and dissipation energies of the system composed of tail rotor and pylon are the sum of the energies of the components. Thus,

$$\begin{aligned} T &= T_1 + T_2 + T_p \\ U &= U_1 + U_2 + U_p \\ F &= F_1 + F_2 + F_p \end{aligned} \tag{6}$$

The generalized Lagrangian form of the equations of motion is

$$\frac{d}{dt}\left(\frac{\partial T}{\partial \dot{q}}\right) - \frac{\partial T}{\partial q} + \frac{\partial U}{\partial q} + \frac{\partial F}{\partial \dot{q}} = F_q(t)$$

where q is the generalized coordinate of interest and $F_q(t)$ is the externally applied forcing function.

$$F_x(t) = F_y(t) = 0$$

$$F_{\zeta_i}(t) = (-1)^i g S_b \cos(\psi+\zeta_i) \tag{7}$$

Substituting the energy and forcing expressions into the Lagrangian form, linearizing, and assuming small angular blade motions result in the following equations of motion:
for the pylon,

$$M_x\ddot{x} + D_x\dot{x} + K_x x + S_b(-\ddot{\zeta}_1 \sin\psi - 2\Omega\dot{\zeta}_1 \cos\psi + \zeta_1\Omega^2 \sin\psi + \ddot{\zeta}_2 \sin\psi + 2\Omega\dot{\zeta}_2 \cos\psi - \zeta_2\Omega^2 \sin\psi) = 0 \tag{8}$$

$$M_y\ddot{y} + D_y\dot{y} + K_y y + S_b(\ddot{\zeta}_1 \cos\psi - 2\Omega\dot{\zeta}_1 \sin\psi - \zeta_1\Omega^2 \cos\psi - \ddot{\zeta}_2 \cos\psi + 2\Omega\dot{\zeta}_2 \sin\psi + \zeta_2\Omega^2 \cos\psi) = 0$$

and for the blades,

$$I_b\ddot{\zeta}_1 + D_b\dot{\zeta}_1 + K_b\zeta_1 + S_b(-\ddot{x} \sin\psi + \ddot{y} \cos\psi + e\Omega^2\zeta_1) = -gS_b(\cos\psi - \zeta_1 \sin\psi) \tag{9}$$

$$I_b\ddot{\zeta}_2 + D_b\dot{\zeta}_2 + K_b\zeta_2 + S_b(\ddot{x} \sin\psi - \ddot{y} \cos\psi + e\Omega^2\zeta_2) = gS_b(\cos\psi - \zeta_2 \sin\psi)$$

Some simplification can be obtained by combining the blade motions. Let

$$\theta_o = \zeta_1 + \zeta_2$$

$$\theta_1 = \zeta_1 - \zeta_2 \tag{10}$$

Then, summing the equations for blade motion results in

$$I_b\ddot{\theta}_o + D_b\dot{\theta}_o + I_b\omega_b^2\,\theta_o = gS_b\theta_1 \sin\psi \tag{11}$$

and taking the difference between the equations for blade motion gives

$$I_b\ddot{\theta}_1 + D_b\dot{\theta}_1 + I_b\omega_b^2\,\theta_1 + 2S_b(\ddot{y}\cos\psi - \ddot{x}\sin\psi) = gS_b\theta_o \sin\psi - 2gS_b\cos\psi \tag{12}$$

where,

$$\omega_b^2 = \frac{K_b + eS_b\Omega^2}{I_b}$$

The equations of pylon motion then become

$$M_x\ddot{x} + D_x\dot{x} + K_x x + S_b(-\ddot{\theta}_1 \sin\psi - 2\Omega\dot{\theta}_1\cos\psi + \Omega^2\theta_1\sin\psi) = 0$$

$$M_y\ddot{y} + D_y\dot{y} + K_y y + S_b(\ddot{\theta}_1\cos\psi - 2\Omega\dot{\theta}_1\sin\psi - \Omega^2\theta_1\cos\psi) = 0 \tag{13}$$

It is noteworthy that the θ_o - equation, which describes in-phase motion of the blades (i.e., motions in the same rotational direction), is very nearly decoupled from the three remaining equations. Coupling occurs only with the θ_1 - equation, which describes out-of-phase motion of the blades (i.e., motions in opposite rotational directions); this is a result of the steady force (gravity) excitation. The set of linear equations with periodic coefficients was solved on an Electronics Associates model 231R analog computer. The analog computer patchboard schematic is shown in Figure 5. In order to scale the problem it was necessary to expand the time scale such that $\sqrt{10^5}$ seconds of computer time corresponded to one second of real time. The scale factors used for the analog variables are given in Table IV.

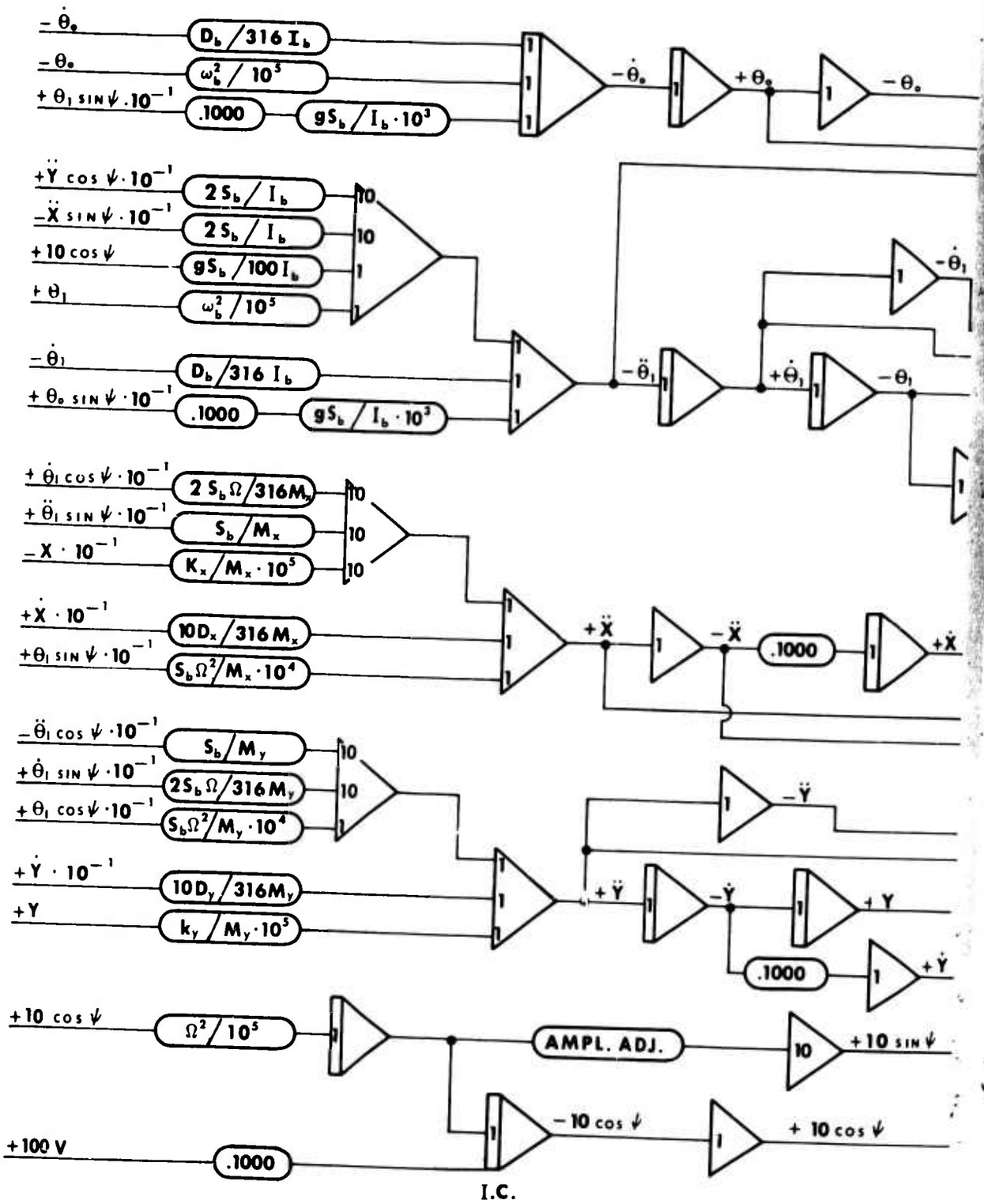

Figure 5. Analog Computer Patchboard Schematic.

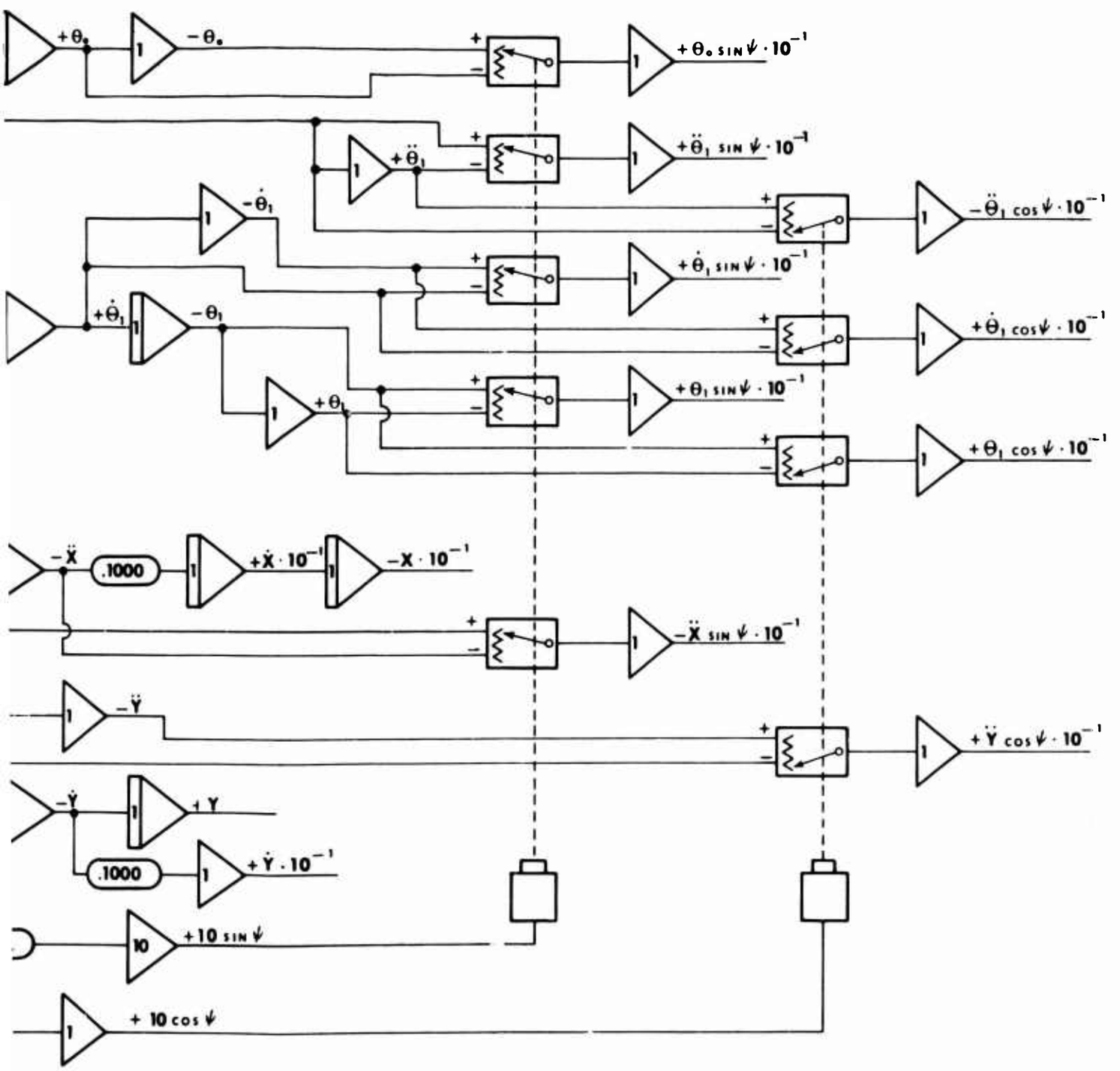

Schematic.

11019-69

TABLE IV. ANALOG COMPUTER SCALE FACTORS

Variable	UH-1D Tail Rotor and Pylon	GRP Tail Rotor on whirl Test Rig	GRP Tail Rotor on UH-1D Pylon
x	.00002 ft/volt	.0002 ft/volt	.0002 ft/volt
$\dot{x}$	.00632 ft/sec/volt	.0632 ft/sec/volt	.0632 ft/sec/volt
$\ddot{x}$	2.0 ft/sec^2/volt	20.0 ft/sec^2/volt	20.0 ft/sec^2/volt
y	.00002 ft/volt	.0002 ft/volt	.0002 ft/volt
$\dot{y}$	.00632 ft/sec/volt	.0632 ft/sec/volt	.0632 ft/sec/volt
$\ddot{y}$	2.0 ft/sec^2/volt	20.0 ft/sec^2/volt	20.0 ft/sec^2/volt
θ_o	.00002 rad/volt	.0002 rad/volt	.0002 rad/volt
$\dot{\theta}_o$	.00632 rad/sec/volt	.0632 rad/sec/volt	.0632 rad/sec/volt
$\ddot{\theta}_o$	2.0 rad/sec^2/volt	20.0 rad/sec^2/volt	20.0 rad/sec^2/volt
θ_1	.00002 rad/volt	.0002 rad/volt	.0002 rad/volt
$\dot{\theta}_1$	.00632 rad/sec/volt	.0632 rad/sec/volt	.0632 rad/sec/volt
$\ddot{\theta}_1$	2.0 rad/sec^2/volt	20.0 rad/sec^2/volt	20.0 rad/sec^2/volt

CHECKS ON THE VALIDITY OF THE MATHEMATICAL MODEL

Fundamental vertical and longitudinal natural frequencies at the tail rotor gearbox output shaft were obtained experimentally during run-up of a UH-1D and by impact tests. The effective mass in each direction was estimated. For conservatism, the effective mass longitudinally was assumed to be only the tail rotor and its gearbox. In the vertical direction, the structural portion of the tail rotor pylon was assumed to contribute to the effective mass. In order to establish the validity of both the equations of motion and the dynamic characteristics of the UH-1D tail rotor mount, the initial analog solutions were obtained for the standard UH-1D tail rotor. The blade mass and stiffness characteristics for this rotor were obtained from Reference 6. These were used to calculate the blade fundamental in-plane mode shape and bending frequency as a function of rotor speed and for rigidly mounted axle, as shown in Figures 6 and 7. The numerical values of the parameters used to represent the UH-1D in this mathematical model are given in Table V.

Solutions were obtained for several discrete rotor speeds in the run-up to operating range. The amplitudes of the pylon motion at the tail rotor gearbox could not be correlated because the influence of the main rotor on the experimentally determined gearbox motion lead to considerably higher amplitude motions than the tail rotor alone would have generated. However, correlation of the vertical and horizontal frequencies of the pylon motion at the tail rotor gearbox with those obtained experimentally was excellent. The equations of motion and numerical values of the parameters used were thus considered to be representative of the UH-1D tail rotor mount.

It should be noted that both the blade and the tail rotor pylon motions computed for the UH-1D configuration, with gravity excitation, were very small and indicated lack of either resonant or self-excited conditions. The in-phase motion of the blades was negligible. The out-of-phase motion of the blades occurred fundmaentally at one-per-rev frequency, with evidence of some two-per-rev included when the rotor speed was in the operating range. The blade motion amplitude did not exceed .01 degree throughout the speed range considered. The pylon vertical motion consisted of oscillations at the pylon fundamental vertical frequency of $8\frac{1}{2}$ cps, upon which were impressed two-per-rev oscillations due to the tail rotor. The pylon longitudinal motion consisted of two-per-rev oscillations, upon which were impressed the pylon fundamental longitudinal frequency of 160 cps. The pylon motions were extremely small in both the vertical and longitudinal directions. The longitudinal motion was essentially nonexistent until the rotor speed was in the operating range ($N_r \geq 85\%$); this is corroborated by the experimental evidence.

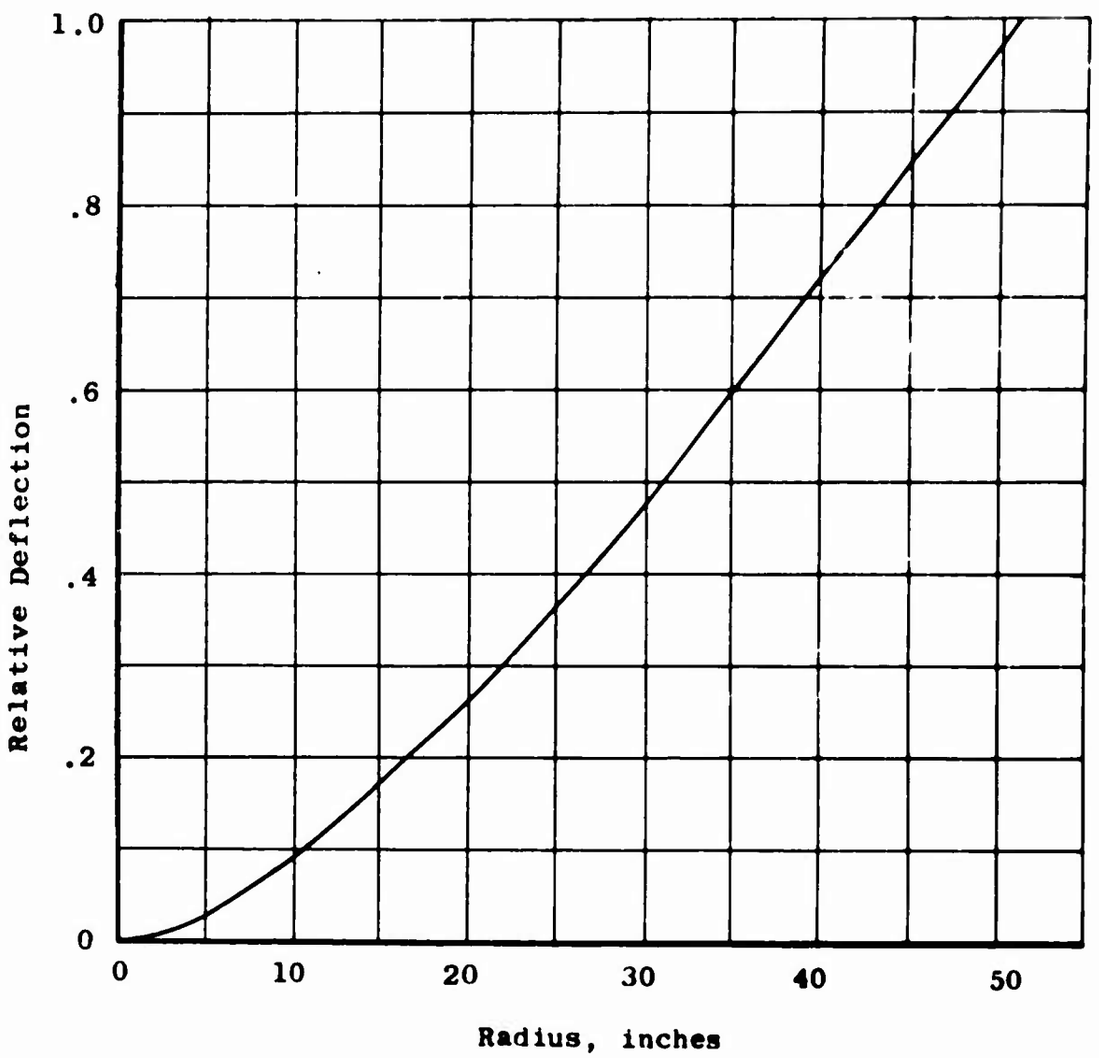

Figure 6. First In-Plane Bending Mode Shape of UH-1D Tail Rotor Blade.

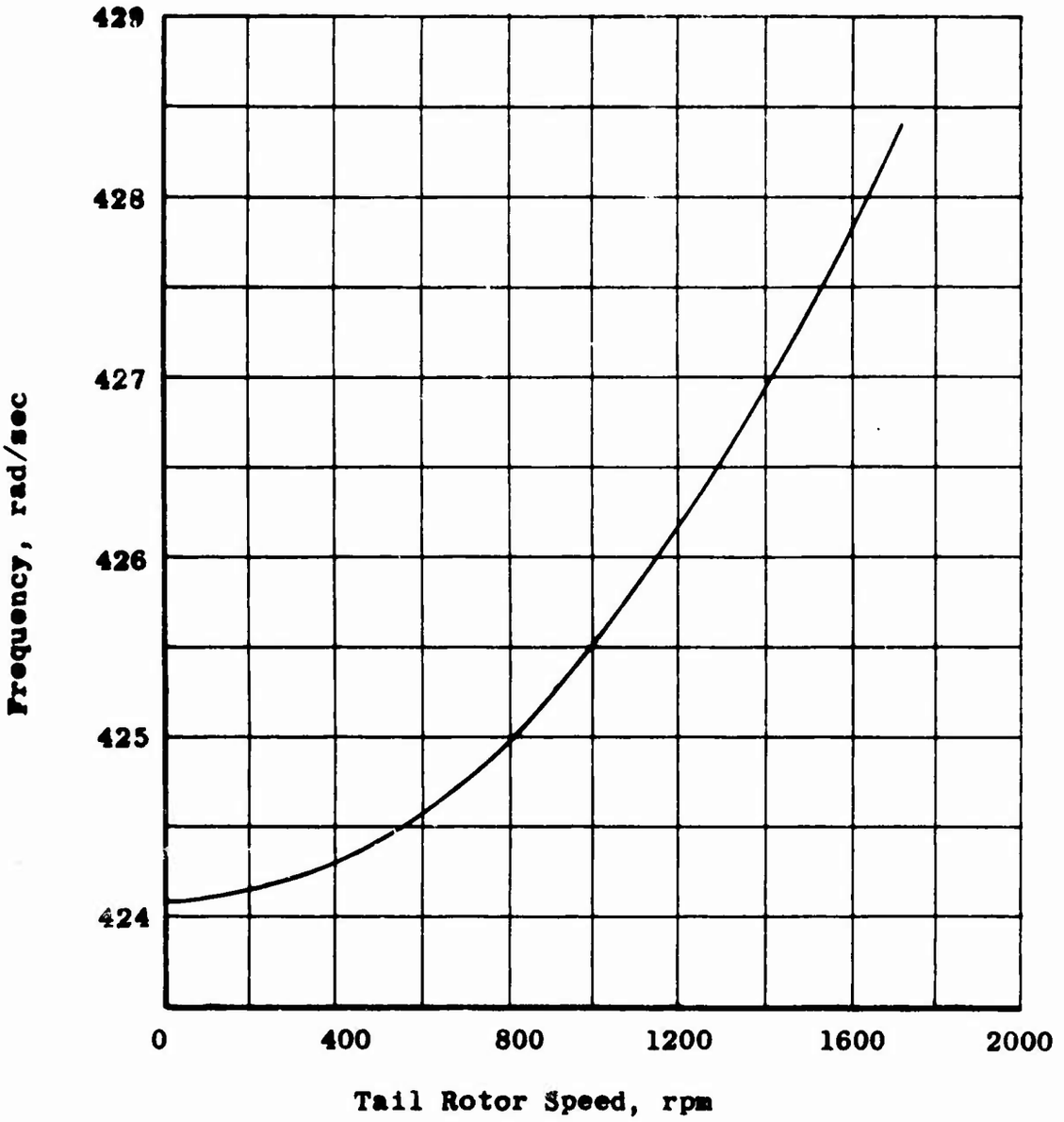

Figure 7. First In-Plane Bending Frequency of UH-1D Tail Rotor Blade.

TABLE V. PARAMETERS USED IN MATHEMATICAL MODELS

Parameter	UH-1D Tail Rotor and Pylon		GRP Tail Rotor on Whirl Test Rig		GRP Tail Rotor on UH-1D Pylon	
I_b	1.165	slug-ft^2	.862	slug-ft^2	.862	slug-ft^2
D_b/I_b	.04 Ω	1/sec	.08 Ω	1/sec	.08 Ω	1/sec
k_b/I_b	179,000.	1/sec^2	6,162.	1/sec^2	6,162.	1/sec^2
e	.261	ft	.335	ft	.335	ft
S_b/I_b	.426	1/ft	.424	1/ft	.424	1/ft
M_x	1.620	slugs	1.650	slugs	1.471	slugs
D_x/M_x	200.	1/sec	.08 Ω	1/sec	200.	1/sec
k_x/M_x	10^6	1/sec^2	79,000.	1/sec^2	10^6	1/sec^2
M_y	2.401	slugs	1.650	slugs	2.252	slugs
D_y/M_y	.08 Ω	1/sec	.08 Ω	1/sec	.08 Ω	1/sec
k_y/M_y	2,840.	1/sec^2	79,000.	1/sec^2	2,840.	1/sec^2

As a further check on the equations of motion, solutions were obtained for the reinforced plastic tail rotor as mounted on the tail rotor whirl test stand. The blade's fundamental in-plane mode shape and bending frequency, as a function of rotor speed and for rigidly mounted axle, are shown in Figures 8 and 9. The natural frequency of the whirl rig stand was determined by impact test for various simulated rotor weights. Thus, the frequencies and effective masses in both the longitudinal and vertical directions were readily determined. In this respect, the test rig was found to be essentially isotropic, having, within the accuracy of experimental error, the same frequency and effective mass in the longitudinal and vertical directions. The numerical values of the parameters used to represent the whirl rig and glass reinforced plastic tail rotor in this mathematical model are given in Table V.

Solutions were obtained for several discrete rotor speeds in the run-up to overspeed range. The vibratory in-plane deflections of the rotor blades, as a function of rotor speed, are shown in Figure 10. Although the magnitude of the bending moment which these deflections represent cannot be compared directly with the vibratory edgewise moments recorded during experimental rotor run-up and reported in Reference 1, the trend exhibited by the vibratory deflection compares favorably with the trend of the vibratory moments. The slight discrepancy in the rotor speed at which the peak steady force resonance occurs is probably attributable to minor discrepancies in the blade and whirl rig frequencies, used in the mathematical model, as compared to the actual frequencies. The favorable comparison of the widths of the theoretical and experimental resonant peaks indicates that the values of structural damping used in the mathematical model were essentially correct. The in-phase blade motion was negligible. The out-of-phase blade motion occurred at essentially one-per-rev, but it was not a well-defined simple harmonic motion for rotor speeds below resonance. As would be expected for the case of isotropic supports, the whirl stand moved equally in the vertical and longitudinal directions. The motions occurred at two-per-rev and remained small even during the rotor resonance. It appears that the buildup in blade motion amplitude, which is present as the rotor speed is increased through the operating range and into the overspeed condition, is indicative of the approach of the second steady force resonance.

It appears from these solutions that the mathematical representation of the glass reinforced plastic tail rotor was sufficiently accurate to lend credence to similar calculations in which the tail rotor was mounted on the UH-1D tail rotor pylon.

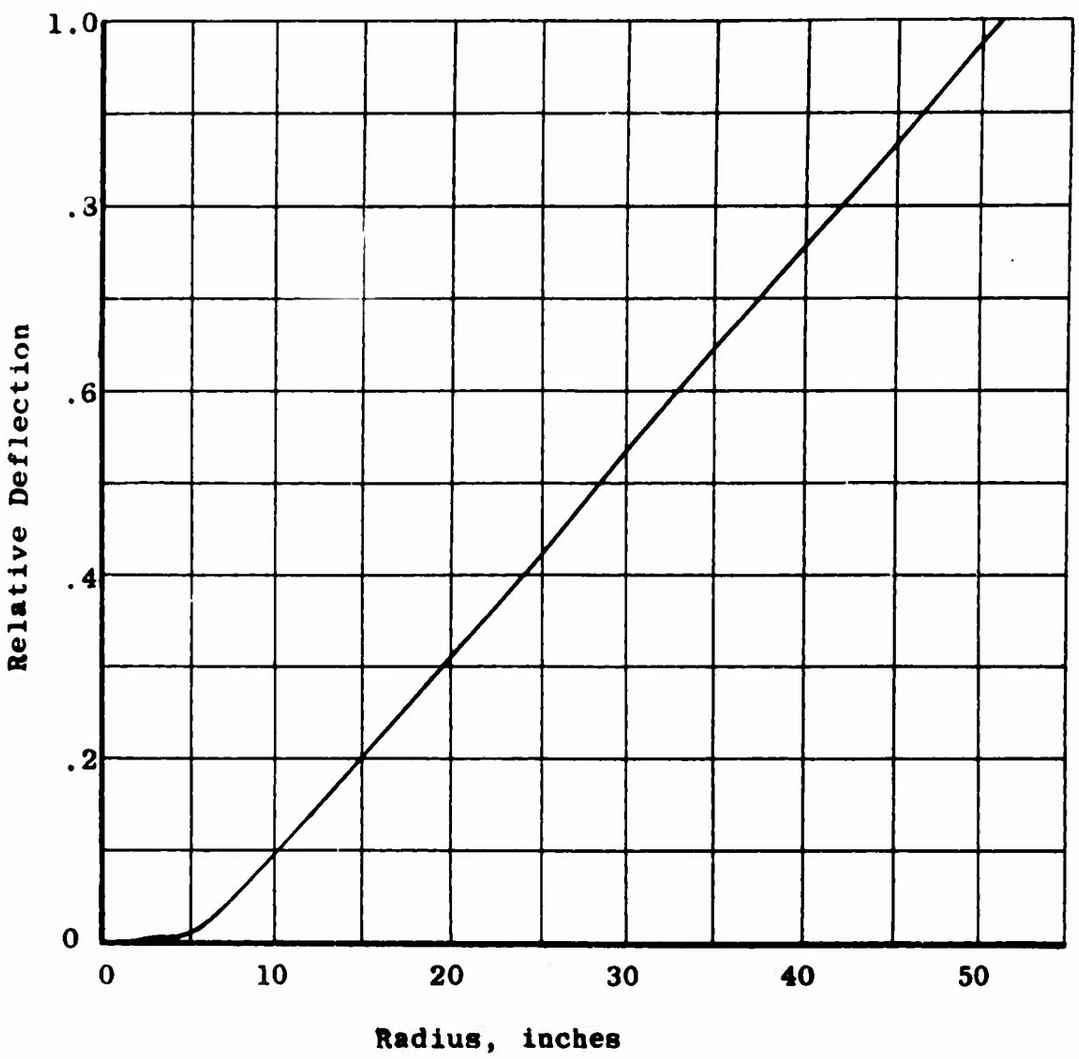

Figure 8. First In-Plane Bending Mode Shape of Glass Reinforced Plastic Tail Rotor Blade.

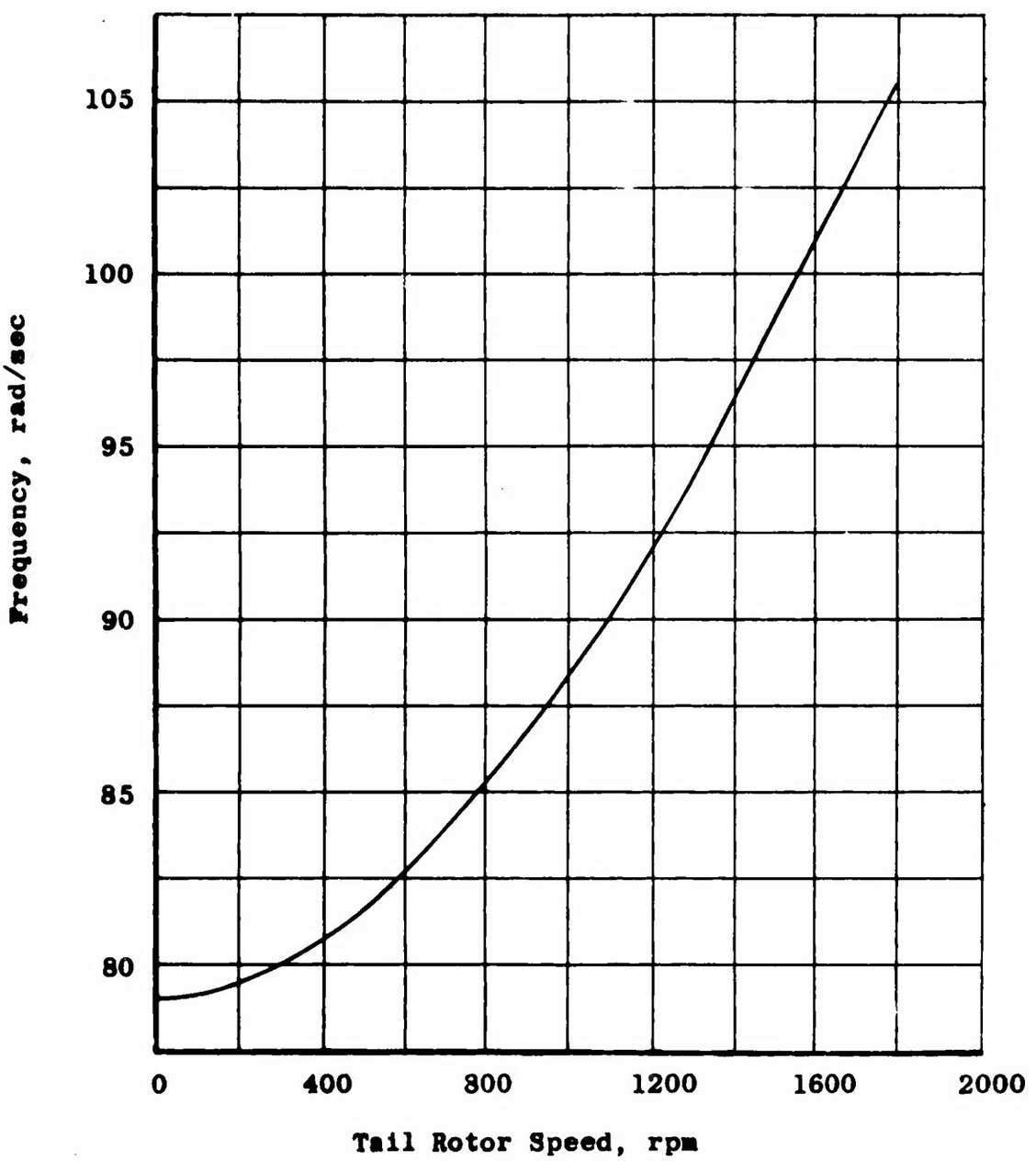

Figure 9. First In-Plane Bending Frequency of Glass Reinforced Plastic Tail Rotor Blade.

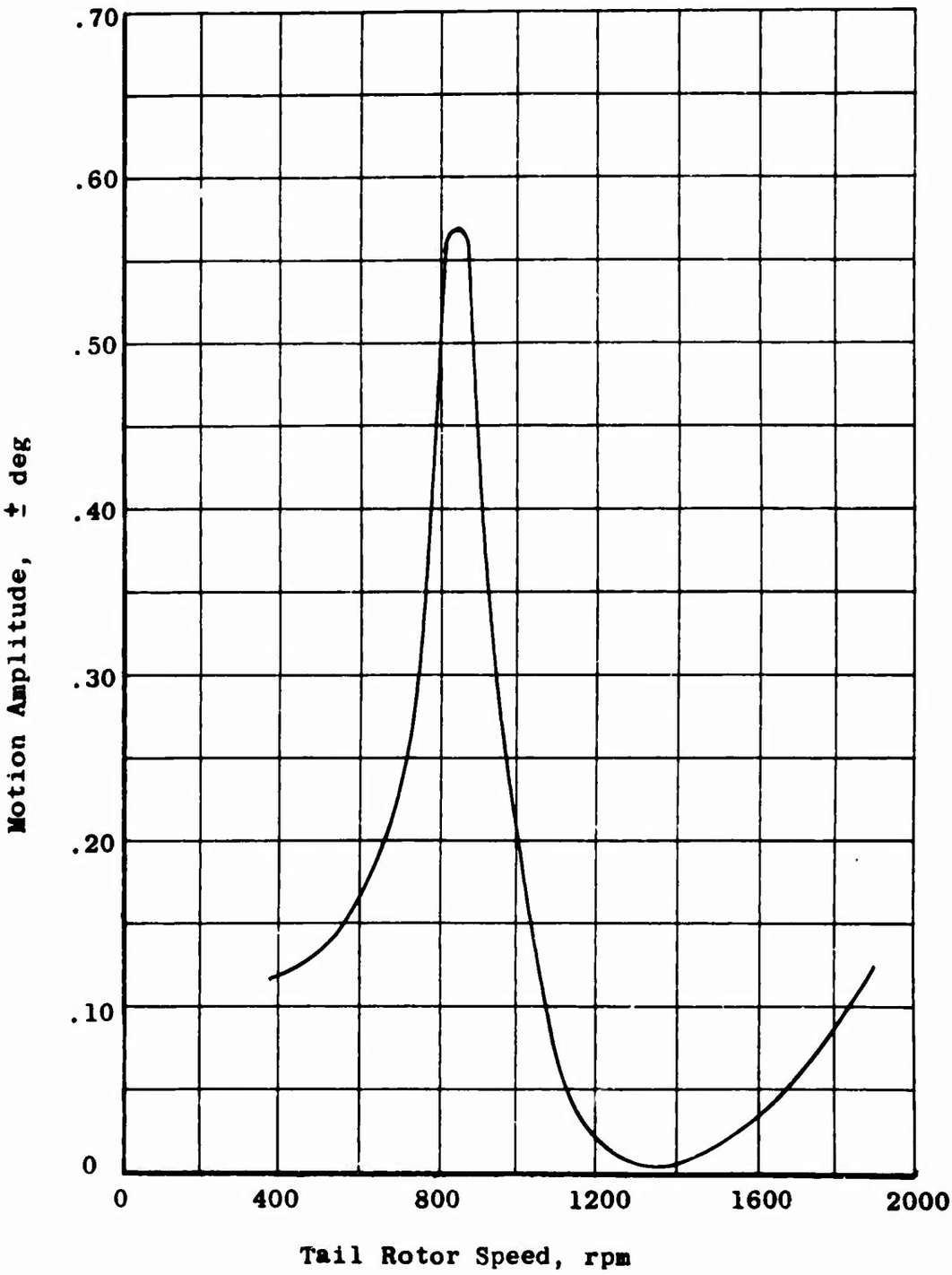

Figure 10. Vibratory Motion of Glass Reinforced Plastic Tail Rotor Blade Mounted on Whirl Rig.

RESULTS OF GLASS REINFORCED PLASTIC TAIL ROTOR ON UH-1D PYLON

The numerical values of the parameters used to represent the glass reinforced plastic tail rotor mounted on the UH-1D tail rotor pylon are given in Table V. Solutions were obtained for several discrete rotor speeds in the run-up to overspeed range. The vibratory in-plane deflections of the rotor blades, as a function of rotor speed, are shown in Figure 11. These results indicate the occurrence of a steady force resonance at a somewhat higher rotor speed than was present on the whirl test rig. It is noteworthy, however, that the resonance occurs at a rotor speed well below the operating range of the tail rotor. Further, the peak amplitude of motion is only approximately 13% greater than that encountered on the whirl test rig. This indicates that the bending moments encountered in going through resonance during run-up and shutdown will not affect rotor life. The in-phase blade motion was negligible. The out-of-phase motion was a well-defined sinusoidal one-per-rev for rotor speeds above the resonance. At rotor speeds below the resonance, the motion was essentially one-per-rev, but it was not a well-defined simple harmonic motion. The pylon motions followed much the same pattern, with variations in rotor speed, as were computed using the standard UH-1D tail rotor. The pylon motions were somewhat larger as a result of the larger blade excursions, but they can be considered to be very small, less than .05 inch, compared to blade motions. There exists no evidence of impending second steady force resonance even at the overspeed condition of 1900 RPM.

It is apparent, from the results shown in Figure 11, that the glass reinforced plastic tail rotor is free of any tendency to exhibit self-excited whirling or self-excited vibrations up to 1900 RPM when mounted on the UH-1D tail rotor pylon. This can be attributed to the extremely anisotropic nature of the pylon. The lack of symmetry leads to motions which are not conducive to self-excited whirling during operation of the low-stiffness tail rotor on the vertically soft pylon. Operation of the glass reinforced plastic tail rotor on the UH-1D thus appears to be entirely feasible from the standpoint of self-excited vibrations, self-excited whirling, and steady force resonance.

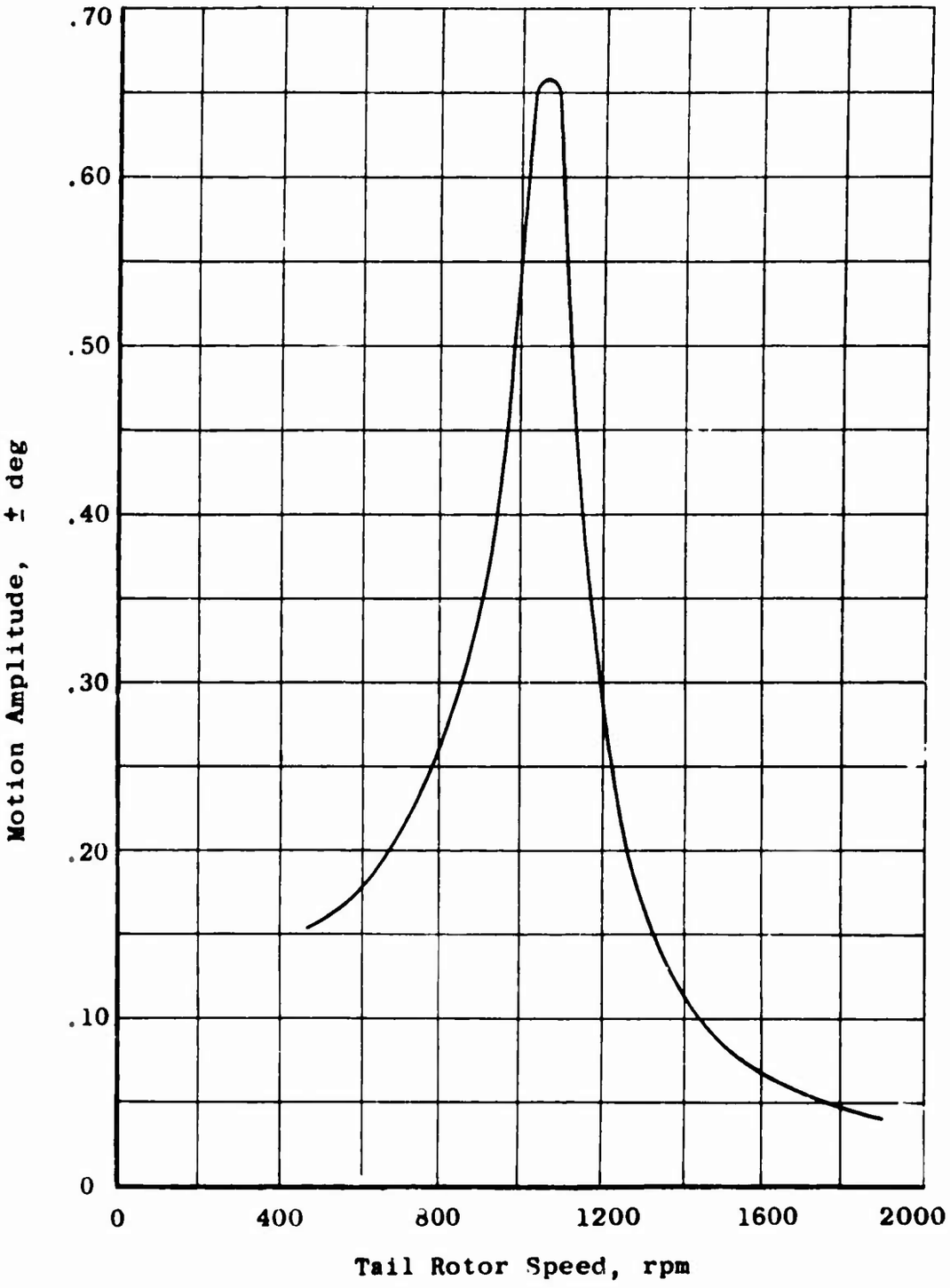

Figure 11. Vibratory Motion of Glass Reinforced Plastic Tail Rotor Blade Mounted on UH-1D.

CONCLUSIONS

It is concluded that:

1. The glass fiber reinforced plastic tail rotor will encounter vibratory loads in forward flight that are within the capability of spar strength, and the rotor will therefore have a high fatigue life.

2. The tail rotor developed during this program has been successfully whirled at full pitch and subsequently to overspeed and has therefore passed many of the more rigorous requirements of operational rotors.

3. The dynamics of the rotor when mounted on a UH-1D helicopter tail boom will not adversely affect operations.

4. Production of the critical element of the rotor can be readily automated by a unique "Pull-Trusion" method which will yield high-quality low-cost spars.

RECOMMENDATIONS

Since it has been concluded that the rotor developed during this program has met many of the substantiation requirements of operational rotors, it is recommended that this concept be carried to an advanced development stage, where its full potential as a flightworthy article can be examined.

LITERATURE CITED

1. Maloney, Paul F., Clark, Frank B., and McIntyre, Hugh H., APPLICATION OF DIRECTED GLASS FIBER REINFORCED PLASTIC TO HELICOPTER TAIL ROTOR ASSEMBLY, R-717, Kaman Aircraft Division of Kaman Corporation, Bloomfield, Connecticut; USAAVLABS Technical Report 68-29, U.S. Army Aviation Materiel Laboratories, Fort Eustis, Virginia, June 1968.

2. Saffire, Victor N., et al., APPLICATION OF ADVANCED FIBROUS REINFORCED COMPOSITE MATERIALS, General Electric Co.; AFML Technical Report 66-272 Vol. II, Air Force Materials Laboratory, Wright-Patterson Air Force Base, Ohio, September 1966.

3. Rogers, C.W., Thornton, H.R., APPLICATION OF ADVANCED FIBROUS REINFORCED COMPOSITE MATERIALS TO AIR FRAME STRUCTURES, General Dynamics, Fort Worth, Texas; AFML Technical Report 66-313 Volume III, Air Force Materials Laboratory, Wright-Patterson Air Force Base, Ohio, September 1966.

4. Wilson, Frank, RESEARCH ON RESIN-IMPREGNATED, COLLIMATED BORON FILAMENTS AND IMPROVED HIGH-MODULUS, HIGH-STRENGTH FILAMENTS AND COMPOSITES, Whittaker Corp, San Diego, California; AFML Technical Report 67-20, Air Force Materials Laboratory, Wright-Patterson Air Force Base, Ohio, January 1967.

5. Coleman, Robert P., and Feingold, Arnold M., THEORY OF SELF-EXCITED MECHANICAL OSCILLATIONS OF HELICOPTER ROTORS WITH HINGED BLADES, NACA TN 3844, February 1957.

6. Wagner, F.J., TAIL ROTOR HUB AND BLADE ASSEMBLY AND ROTATING CONTROLS ANALYSIS FOR THE ADVANCED UTILITY HELICOPTER YHU-1D and HU-1B, Bell Helicopter Company, Report No. 204-099-262, Fort Worth, Texas, January 1960.

Unclassified
Security Classification

DOCUMENT CONTROL DATA - R & D

(Security classification of title, body of abstract and indexing annotation must be entered when the overall report is classified)

1. ORIGINATING ACTIVITY (Corporate author)
Kaman Aircraft, Division of Kaman Corporation
Old Windsor Road
Bloomfield, Connecticut

2a. REPORT SECURITY CLASSIFICATION
Unclassified

2b. GROUP

3. REPORT TITLE
STUDY AND EVALUATION OF DIRECTED GLASS FIBER REINFORCED PLASTIC HELICOPTER TAIL ROTOR ASSEMBLY

4. DESCRIPTIVE NOTES (Type of report and inclusive dates)
Final Report

5. AUTHOR(S) (First name, middle initial, last name)
Paul F. Maloney
Frank B. Clark
Hugh H. McIntyre

6. REPORT DATE
October 1969

7a. TOTAL NO. OF PAGES
56

7b. NO. OF REFS
6

8a. CONTRACT OR GRANT NO
DA 44-177-AMC-306(T)

b. PROJECT NO.
Task 1F162203A14176

c.

d.

9a. ORIGINATOR'S REPORT NUMBER(S)
USAAVLABS Technical Report 69-43

9b. OTHER REPORT NO(S) (Any other numbers that may be assigned this report)
Kaman Aircraft Report R-774

10. DISTRIBUTION STATEMENT
This document is subject to special export controls, and each transmittal to foreign governments or foreign nationals may be made only with prior approval of US Army Aviation Materiel Laboratories, Fort Eustis, Virginia 23604.

11. SUPPLEMENTARY NOTES

12. SPONSORING MILITARY ACTIVITY
US Army Aviation Materiel Laboratories
Fort Eustis, Virginia

13. ABSTRACT

The results of study and evaluation of a new design concept for helicopter tail rotors are reported. The evaluation was conducted by means of a whirl test which included separate runs at full pitch (19°), overspeed to 110% rpm, and simulated forward flight to 105 knots. The dynamics of this rotor mounted on an Army helicopter and the techniques for automating its production were subjects of separate study phases for this program.

Sufficient development work has been accomplished to demonstrate not only that the basic concept is feasible but that the rotor built in this program is capable of surpassing many of the more rigorous substantiation requirements of operational helicopter rotors. Also techniques are available for the volume production of such a rotor to high quality standards at low cost.

DD FORM 1 NOV 68 1473 REPLACES DD FORM 1473, 1 JAN 64, WHICH IS OBSOLETE FOR ARMY USE.

Unclassified
Security Classification

14. KEY WORDS	LINK A		LINK B		LINK C	
	ROLE	WT	ROLE	WT	ROLE	WT
Helicopter						
Tail Rotor						
Fiberglass						
Automation						
Whirl Test						